Remote Sensing in Hydrogeology:

A short summary of methods and constraints for groundwater exploration

Lorenz Wendt[1], Sylke Hilberg[2], Jörg Robl[2], Daniel Dirnberger[2], Thomas Strasser[1], Andreas Braun[3]

[1]Interfaculty Department of Geoinformatics Z_GIS, University of Salzburg, Austria

[2]Department of Geography and Geology, University of Salzburg, Austria

[3]Department of Geography, University of Tübingen, Germany

31. March 2016

This documentation has been prepared as Deliverable 5.1 in the project *EO4HumEn - Earth Observation based services to support humanitarian operations: monitoring population and natural resources in refugee/IDP camps*, funded by the Austrian Research Promotion Agency FFG (ASAP 9, Nr. 840081). Further information on this project can be found at www.zgis.at/humanitarian-services

TABLE OF CONTENTS

PURPOSE AND SCOPE OF THIS DOCUMENT

One aim of the EO4HumEn project is the exploration for potential groundwater borehole sites for the supply of refugee and IDP (internally displaced persons) camps with drinking water. Information on the geological and hydrological situation in adequate detail is essential to assess valuable drilling sites, which is often missing or unavailable. Remote sensing is useful to gather the required information in a reasonable timeframe by greatly reducing the amount of fieldwork. Geological mapping aiming on lithology and hydrogeology is a well-established application of remote sensing. Several textbooks have been written on this topic, including Gupta (1991), "Remote Sensing Geology", and Prost (2002), "Remote Sensing for Geologists". Another valuable source is Meijerink et al. (2007), "Remote Sensing Applications to Groundwater".

This document represents a highly condensed, practical guideline for the production of remote-sensing based hydrogeological reconnaissance maps and it is not the intention to replace these excellent and comprehensive introductions to remote sensing techniques and applications mentioned above. The indented readership consists of remote sensing practitioners and hydro-geologists, which require a concise and tangible guideline on state of the art methods and required datasets to achieve a best practice hydrological characterization of a given study area. Textbook examples are often selected due to their simplicity, which can result in a bias concerning the possibilities and limitations of remote sensing for groundwater. Groundwater is, by its nature, a subsurface phenomenon, hidden to the exploration by the view from above. This document displays a more realistic picture by giving example cases from various climatic and geological settings. Some of the geological settings presented in this document are fairly simple, and provide excellent outcrop conditions, so that a reconnaissance map based on remote sensing is sufficient to determine suitable drilling sites for groundwater extraction; in other cases, the outcome of the remote sensing study can only act as a basis for thorough field work and geophysical investigations.

The text is structured as following: Chapter 1 provides a very compact introduction and guideline to the reasoning behind the exploration for groundwater in different geological settings. As a summary, the elements of the intended product of groundwater exploration, which is a hydrogeological reconnaissance map, are listed. The available datasets and methods to derive these elements are explained in a best practice guide in chapter 2. Finally, chapter 3 provides examples from areas characterized by different geological settings, climatic zones and outcrop conditions.

This document is part of the project EO4HumEn, a joint project of the Department of Geoinformatics Z_GIS, University of Salzburg, Doctors without Borders Section Austria, and the Department of Geography and Geology, University of Salzburg. The aim of this project was to further develop Earth-observation based methods to support humanitarian action in three domains: (1) the estimation of population numbers in refugee and IDP camps using very highly resolved satellite images and object-based image analysis; (2) the support of groundwater exploration by remote sensing, and (3) the assessment of changes of the environment around refugee/IDP camps. The project

lasted from October 2013 to March2016 and was funded by the Austrian Research Promotion Agency FFG. The developed products and services continue to be offered by Z_GIS to humanitarian actors (www.zgis.at/humanitarian-services).

1 A SHORT INTRODUCTION TO GROUNDWATER GEOLOGY

Before starting with the discussion of groundwater flow in different rock types, it may be helpful to define a few basic terms. *Permeability* is the material property of a subsurface material, which describes the ability of fluids (gas or liquids) to pass through it, and thus describes solely the material itself. *Conductivity* describes the ability of a specific fluid to pass through the subsurface material, and thus depends both on the subsurface material and the fluid. *Transmissivity* describes the conductivity of the specific subsurface body, and thus depends on the material's properties, fluid's properties, the geometry and the internal structure of the subsurface body. An *aquifer* is a groundwater containing subsurface body, which has a high permeability, an *aquiclude* is a basically impermeable subsurface body.

The groundwater flow takes place in the voids of the subsurface material. In unconsolidated sediments and clastic, homogeneous sedimentary rocks these voids are pores which make up the *primary porosity* or *matrix porosity.* These types of aquifers are denoted as *porous aquifers.* In consolidated sedimentary rocks and crystalline rocks voids are made by structures such as fractures, faults or foliations. These structures are also summarized as *secondary porosity.* As crystalline and consolidated sedimentary rocks are also named *hard rocks*, aquifers in these rock types are often referred to as *fractured hard rock aquifers*. The hydraulic conditions in these two general types of aquifers are completely different.

Porous aquifers differ by their grain-size distributions, which are a result of the depositional processes forming these deposits. Fluvial sediments consist of coarse-grained sediments such as sands and gravels, show high hydraulic conductivities and thus are more suitable as drinking water reservoirs than fine grained lacustrine or eolian sediments with a significantly lower hydraulic conductivity. In porous aquifers groundwater fills the pores between grains and can be found anywhere within the water bearing layer. Thus, the decision for potential drilling sites for drinking water supply is mainly controlled by the regional and local flow direction with respect to potential pollutants.

Fractured hard rock aquifers involve a wide range of hydraulic conditions due to lithological variations and deformation history. In intrusive or metamorphic rocks groundwater flow is limited to fractures. In sedimentary rocks such as sandstones a combination of fractures and matrix porosity may be responsible for groundwater flow. The decision for potential borehole sites in fractured aquifers is governed by the location of boundaries between aquifers and aquicludes, and brittle structures like faults or fractures, which can be recognized as lineaments in satellite images under favorable conditions.

In carbonatic rocks (limestones, dolomite rocks), *karstification* is the most important factor that determines hydraulic conductivity. Karstification is the process of dissolution of carbonatic rocks over geological time scales by groundwater. The acidity is caused by CO_2 dissolved in the water. Karstification can cause few, very effective groundwater conduits in the limestone, so that groundwater exploration has to target these conduits. Karst aquifers are also particularly vulnerable to pollution, because these conduits can transport pollutants very quickly

from their source to an abstraction site, with very little filtering in between. Karst structures at the surface can be mapped by remote sensing.

Table 1: Recommended workflow for hydrogeological reconnaissance mapping

<table>
<tr><td rowspan="2">1</td><td colspan="6">Type of aquifer
• Topography
• Hard rock outcrops
• Regional Geology</td></tr>
<tr><td colspan="3">Porous aquifer</td><td colspan="3">Fractured aquifer</td></tr>
<tr><td rowspan="2">2</td><td colspan="3">Types of Deposits</td><td colspan="3">Lithology</td></tr>
<tr><td>Fluvial sediments</td><td>Lacustrine sediments</td><td>Eolian sediments</td><td>Crystalline rocks</td><td>Clastic, sedimentary or volcanic rocks</td><td>Carbonatic rocks</td></tr>
<tr><td>3</td><td colspan="3"></td><td colspan="2">Lineament analysis, fold mapping
• Brittle or ductile structures
• Hydraulic properties of fractures
• Hydraulic properties of layer boundaries</td><td>• Karst landforms</td></tr>
<tr><td>4</td><td colspan="6">Determination of recharge and discharge zones
• Topography
• Surface water bodies, direction of runoff
• Soil humidity
• vegetation</td></tr>
<tr><td>5</td><td colspan="3">Interaction between surface runoff and groundwater
• Seasonal variations
• Flood areas</td><td colspan="3"></td></tr>
<tr><td>6</td><td colspan="6">Potential contaminants
• Settlements
• Camps
• Further influences (e.g., landfills)</td></tr>
<tr><td>7</td><td colspan="6">Roads, borders and other factors that control access to specific sites or areas with a drilling rig</td></tr>
<tr><td>8</td><td colspan="3">Potential borehole site:
Within discharge region, outside of flood areas and upstream of contaminants, which can be easily accessed.</td><td colspan="3">Potential borehole site:
Intersections of water bearing brittle structures (fractures), along layer boundaries or karstified structures, within discharge region and upstream of contaminants, which can be easily accessed.</td></tr>
</table>

Basically, different aquifer types require different investigation methods and adequate levels of information detail, independent of whether hydrogeological field investigations or remote sensing methods are used to understand

groundwater flow and to find potential borehole sites for drinking water exploitation. Any map of the subsurface produced by remote sensing should be considered as an interpretation of image features rather than an actual map of existing bodies and structures before it has been validated in the field. This is especially true in areas with a complex geology and dense vegetation, where the deduction of subsurface phenomena from remote sensing data is particularly challenging.

Table 1 and Figure 1 show the general work flow to select potential drill sites with regard to different geological settings, going from stage 1 to stage 8. Every stage of the investigation demands a combined approach of remote sensing methods and expert based interpretations. The eight steps lead to the elements that a hydrogeological reconnaissance map should finally contain (table 2).

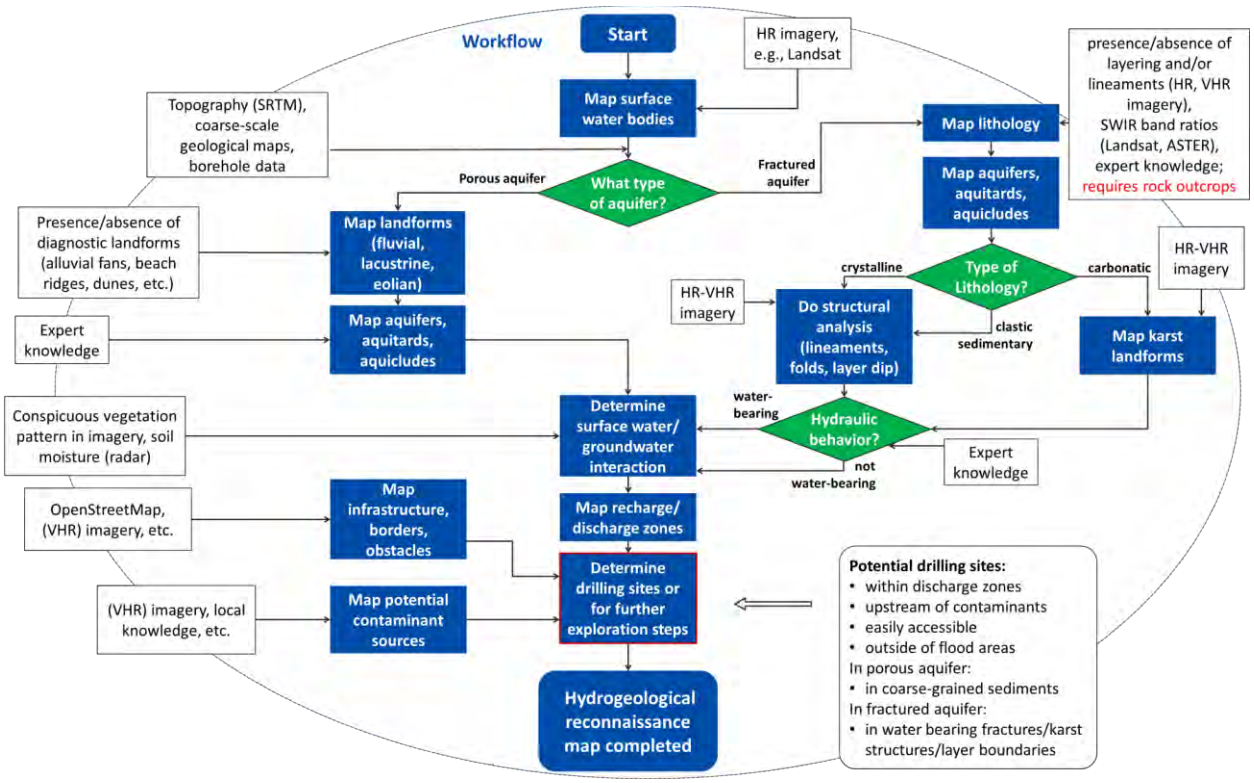

Figure 1: Flow chart for hydrogeological reconnaissance mapping

The most basic distinction to be made is between porous aquifers and fractured aquifers (**stage 1**). This is done based on the topographical inventory of the landscape and the presence of hard rock outcrops. Porous aquifers, consisting of loose sediments, are found in topographically flat areas such as valley floors and coastal plains, and lack significant outcrops of hard rocks. In general, geological maps are usually available at the national or continental scale. Although the level of detail of these maps is low in many cases, it is often sufficient for the general discrimination between porous and fractured aquifers.

In **stage 2**, unconsolidated sediments are further distinguished according to their depositional environment. Although the exact distribution of sediment bodies with different grain sizes and thus permeabilities in the

subsurface cannot be determined by remote sensing, the expected general types of sediments and thus their expected hydrogeological properties differ for the different sedimentary environments. Therefore, a distinction into fluvial deposits (with high overall permeability), lacustrine and eolian deposits (with lower permeability) is useful based on the landforms observed in remote sensing imagery. The corresponding step in hard rock aquifers is the distinction between crystalline rocks (flow along fractures and faults only), clastic sedimentary rocks (flow in pores and fractures), and carbonatic rocks (flow strongly concentrated along few fractures widened by karstification). This step also comprises the determination of the specific lithology by remote sensing, in order to distinguish possible aquifers like sandstones and quartzites from possible aquicludes like, for example, shales.

The next stage (**stage 3**) **is restricted to hard rock terrain** and comprises the mapping of folds and lineaments. Lineaments are linear structures observable in remote sensing data, which are the surface expression of a subsurface phenomenon. Lineaments originated from tectonics are abundant features of the surface of the Earth and give important insights on the deformation history of the investigated region. Such lineaments occur in scales ranging from a few millimeters to several hundred kilometers. Since they may represent preferred fluid pathways they are first order sites for ground water exploration in hard rock domains.

The exploitation of aquifers linked to tectonic structures requires at least some knowledge about the large scale geological setting (preferred orientation of the paleo stress field and related brittle structures) and a deep understanding of structural geology to disentangle brittle from ductile structures that originated at low and high grade metamorphic conditions, respectively. In general, aquifers in hard rock domains are linked to brittle structures with open spaces that promote the channeling and migration of fluid (water) over large distances, while ductile structures like shear zones in high grade metamorphic rocks or even magmatic lineaments like dykes are characterized by extremely low fluid permeability and represent therefore rather fluid barriers than aquifers. An exact characterization of the occurring lineaments by remote sensing and at key areas in the field is required to unravel linear structures of different origin.

In regions that consist of un-metamorphosed sedimentary and low-grade metamorphic rocks the unraveling of potential ground water sites from lineaments is straight forward, as ductile structures are missing and all lineaments that are indicated by long straight linear depressions (caused by the higher erodibility of fractured rocks) are originated from brittle deformation. However, care has to be taken in case of the occurrence of dykes (rare in such a geological setting) that are known to represent fluid barriers. While felsic dykes are generally characterized by a positive topographic expression relative to the host rocks, mafic dykes may feature linear depressions and can therefore be confused with brittle structures so that additional geological information (e.g. mapping in field) is required.

In regions that consist of high grade metamorphic rocks (Sahara Craton, Arabian-Nubian shield, …) the geological situation is even more complicated by the occurrence of crustal scale ductile shear zones and numerous dykes so that the delineation of potential ground water sites mainly by remote sensing becomes challenging. Again, most dykes are characterized by a positive topographic expression caused by a higher erosional resistivity and can

therefore be excluded from potential groundwater exploration sites. Ductile shear zones are characterized by a low fluid permeability and are therefore not suitable for groundwater exploitation. They can be distinguished from brittle structures that may host fertile aquifers by their plan view curvature. While brittle structures follow straight lines, ductile structures feature many curved segments caused by strain gradients and rheology contrasts during the devolvement of shear zones at elevated temperatures (> 350 °C).

Potential ground water exploration sites are therefore located at regions with a high density of large scale, deep reaching, connected and intersecting brittle structures, so that (a) the hydrological drainage area is large enough to provide fertile aquifers without large seasonal discharge oscillations and (b) a long retention time between recharge and discharge to fulfill the quality requirements for drinking water.

The investigation process continues with the determination of recharge and discharge zones (**stage 4**). This comprises a general assessment of the topography to determine the direction of run-off and therefore, the estimated direction of groundwater flow. It also comprises the mapping of permanent and seasonal water bodies like lakes and rivers. In arid or semi-arid regions, the presence of vegetation can be an indicator for groundwater close to the surface, representing discharge zones. Therefore, the production of vegetation index maps or the mapping of soil humidity can be helpful to find suitable groundwater abstraction sites. Known groundwater abstraction sites also have to be mapped.

The interaction between surface waters and groundwater is targeted during **stage 5.** This step includes the mapping of temporarily flooded areas along rivers and shorelines, and other seasonal variations. Multi-temporal satellite imagery, combined with a digital elevation model to find low-lying areas, is employed to this purpose. Temporary lakes without outflow can lead to groundwater infiltration, depending on the surface material and the climatic conditions. Discharge from a groundwater body into a river can be indicated by an increasing width of the river, while no obvious tributaries are observed.

The next step is the mapping of potential groundwater contaminants (**stage 6**). Potential contaminants can be settlements and refugee/IDP camps, where latrines or livestock might introduce pathogens into the groundwater, but also factories, mines, landfills or any other potential sources of pollution.

Drilling of groundwater wells for a refugee/IDP camp or a large village usually requires access with a drilling rig, which is often mounted on or transported by a truck. Therefore, mapping of the existing roads and obstacles and areas that are impassable for ground vehicles should be mapped (**stage 7**). If information on state borders or other access restrictions are known, they should be included in the map product as well.

Finally, in **stage 8**, potential borehole sites can be suggested, when and if the proceeding stages have been successfully terminated. Potential drillsites in areas characterized by porous aquifers are located within a discharge region, outside of flood areas and upstream of contaminants, at locations that can be easily accessed. In fractured aquifers, intersections of water bearing brittle structures represent potential location for field investigations by

geophysical means, and drilling. A potential drilling site has to be located upstream of contaminants and is ideally easily accessible.

Table 2: Elements of a hydrogeological reconnaissance map

Topography: *shaded relief, contour lines*
Lithology: *rock types, classified as aquifer/aquitard/aquiclude; strike and dip of layers*
Folds: *fold axes*
Lineaments: *brittle or ductile, fracture or dyke*
Regional water flow:
Permanent and seasonal water bodies
Recharge and discharge zones: springs, drainage systems
Existing boreholes, water levels, depths, encountered lithology
In porous aquifers: groundwater isohypses, (if known)
Soil moisture (if known from radar)
Vegetation cover
Potential contaminants:
Settlements, camps, industrial installations, etc.
Roads and obstacles
Possible sites for field check and validation
Potential drillsites
Recommended field investigation method

2 BEST PRACTICE GUIDE

2.1 CARTOGRAPHIC SCALE AND PROJECTION

Any mapping project usually starts with the definition of the minimum mapping unit, which is the size of the smallest object that is to be shown on the final map. This, in turn, defines the cartographic scale and the required remote sensing dataset. The general rule is that at least three pixels are required to identity a surface feature in a remote sensing image. For example, if the smallest features to be mapped have a spatial extent of 10 m, satellite imagery with a ground sampling distance (pixel size) of 3 m or smaller is required. In a hydrogeological reconnaissance mapping project there is no simple answer on the question of the appropriate scale and thus, the required imagery. Controlling factors are the geological complexity of the area, the degree of detail of the geological information available in the form of published maps and other material, the extent of the catchment area, the planned yield of the groundwater abstractions (as a larger well will affect a larger area than a smaller one), the pricing of imagery, and the urgency of the study.

If a lithological map has to be created from remote sensing data, the spectral resolution has to allow a distinction of rock types, which is best done with images from Sentinel 2. Landsat and ASTER due to their high spectral resolution, as will be further detailed below. If the lithology is known, but the location of specific features like karst structures is to be mapped, spatially higher resolved imagery might be necessary. On the other hand, geological structures like fractures are often similar across several magnitudes, so that a lineament visible in a coarse image might indicate similar, smaller structures at a finer scale at the same location, which can then be mapped during a field campaign.

From a practitioner's perspective, it is advisable to start with Landsat or Sentinel 2 imagery, which is freely available, and allows the production of maps of up to ~ 1:50.000. This is in many cases detailed enough and allows a comparison to possibly existing geological maps on a local or national scale. As geological features usually do not change much over time, freely available imagery such as that in Google Earth should also be used to map smaller geological features. Also important man-made structures may be detected using Google Earth images, being aware that these structures may not be up to date in all cases. For data exchange and a general applicability the use of the UTM (Universal Transverse Mercator) map projection based on the WGS84 ellipsoid is recommended.

2.2 DATA SOURCES

2.2.1 COMMON DATA SOURCES AND MAPPING SOFTWARE

Data sources

Google Earth: Earth observation data and mapping tool; https://www.google.de/intl/de/earth/

Bing maps: Earth observation data, webmap viewer providing "bird's eye perspective" in four directions, server accessibility (e.g. via ArcGIS Online); http://www.bing.com/maps

Open street map: Community driven open mapped data featuring server accessibility (e.g. via ArcGIS Online); http://www.openstreetmap.org

Global Land Cover 30 (GLC 30) data; http://www.globallandcover.com/GLC30Download/index.aspx

UTM World grid via ArcGIS Online

Mapping software (freeware)

QGIS: http://www.qgis.org/de/site/

Grass-GIS: http://grass.osgeo.org/

SAGA-GIS: http://www.saga-gis.org/

Orfeo toolbox – Monteverdi: http://www.orfeo-toolbox.org/otb/monteverdi.html

Google Earth https://www.google.de/intl/de/earth/

Collection of diverse GIS-freeware: http://fundisa.sansa.org.za/resources%20-%20Open%20Source%20Software.html

2.2.2 GEOLOGICAL AND HYDROGEOLOGICAL BASE MAPS, BOREHOLE DATABASES

The most useful information source would be geological maps, hydrogeological maps or even logs from existing boreholes in the study area. This information is also the most difficult to obtain, because it is not always collected and provided by the national authorities of the country the study site is located in. Therefore, it is impossible to provide a complete list of data sources here. Some interesting sources are the following:

The "onegeology project" lists a number of WMS services for geological maps, and combines them to a global geological web map: www.onegeology.org ; http://portal.onegeology.org/catalogView.jsp

The soil map of Africa: http://eusoils.jrc.ec.europa.eu/esdb_archive/eudasm/africa/indexes/map.htm This website provides some scanned geological and hydrogeological maps of African countries at the national scale.

The United States Geological Survey (USGS) provides a digital geological map of Africa at the continental scale: http://energy.usgs.gov/OilGas/AssessmentsData/WorldPetroleumAssessment/WorldGeologicMaps.aspx

It is also available as a web map service (WMS).

The British Geological Survey (BGS) provides a continental-scale hydrogeological map of Africa: http://www.bgs.ac.uk/research/groundwater/international/africangroundwater/mapsDownload.html

The BGS also maintains an archive on groundwater grey literature for southern Africa: http://www.bgs.ac.uk/sadc/index.cfm

Borehole locations from South Sudan are provided by the Basic Services Fund http://www.bsf-south-sudan.org/. These are not complete and were produced from 2005 to 2008.

Geological and hydrogeological maps of Iraq are available for sale from the Iraq Geological Survey: http://www.geosurviraq.com/

2.2.3 SATELLITE IMAGERY

There are too many sources of satellite remotely sensed data useable for hydrogeological mapping to describe them here in detail and in any case the information will rapidly become outdated. Hence, the focus is on some typical datasets that have been proven in practice and some follow up systems with similar characteristics, but not available yet. A database on satellite missions with detailed descriptions can be found on https://directory.eoportal.org/web/eoportal and a decision chart that gives hints on which data to use for different purposes is offered here http://www.geo-airbusds.com/en/4869-what-product-do-i-choose?n=1806.

In general satellite sensors are characterized by their *geometric* or *spatial resolution* (pixel size of an image representing the recorded area on the ground), *spectral resolution* (covered wavelengths within segments (bands) of the electromagnetic spectrum and number of bands), *radiometric resolution* (refers to the effective bit-depth of the sensor by a number of grayscale levels), and *temporal resolution* (periodicity of recording a given surface location). Satellite image products are often categorized by their spatial resolution, as this defines the representation or visibility of scale dependent real-world objects. The European GMES (Global Monitoring of Environment and Security) data warehouse categorizes very high resolutions (VHR), high resolution (HR) and medium resolution imagery (MR) (details see Table 2-1). For geological applications, MR satellite sensors with large swath sizes are advantageous to VHR sensors due to the availability of large satellite archive, which in fact are substantially cheaper or free of charge.

Table 2-1: Satellite image categorization.

Category	Threshold
VHR1	< 1 m
VHR2	1 – 4 m
HR1	4 – 10 m
HR2	10 – 30 m
MR	30 – 300 m

Remote sensing data can be acquired for different seasons of the year, thereby allowing the temporal variations in reflectance to be exploited for mapping and monitoring purposes. The use of these multi-date image data is particularly beneficial as the degree of spectral distinction between different vegetation types varies across the seasons and for the detection of changes in land cover and landscape composition. For geological surveys satellite data of dry seasons is preferred, as vegetation bias the geological image interpretation. Finding the ideal season for mapping geological features is obviously difficult, but is mostly connected to the climatic conditions within an area. Annual climate charts of an area will give best information for dry to nearly dry seasons. The sun illumination affects the spectral reflectivity of earth surface material. Therefore acquired image quality, determined by the relative sun angle, depends on the latitude / longitude and acquisition date of an area. However, multi-date imagery will possibly always improve satellite image interpretation to a certain extent.

We focus here on satellite data of Landsat series, ASTER data, because they are available free of charge or for a very low price, and provide global archival datasets, which makes the time-consuming tasking of new imagery obsolete. The forthcoming Sentinel-2 dataset is also mentioned here, because it will be available free of charge in the near future. Other potential satellite platforms and sensors are (ordered from VHR to HR) WorldView-3, WorldView-2, Pleiades, GeoEye, Quickbird, SkySat, IKONOS, SPOT 5/6/7, RapidEye, Flock 1 image constellation, ALOS, and others. Satellite data are purchasable via resellers, for example http://www.euspaceimaging.com/, http://www.geo-airbusds.com/geostore/, http://www.e-geos.it, and many others.

The **Landsat program** (5, 7 and 8) is the longest running operation of earth observation from space, where acquired images are available to everybody. Launching the first Landsat satellite platform in 1972, the most recent satellite is Landsat 8 (launched on February 11, 2013). Landsat 8 platform consist of two sensors, namely the Operational Land Imager (OLI) and the Thermal InfraRed Sensor (TIRS), which differ in the spectral range and geometric resolution. OLI collects data from nine spectral bands, whereas the geometric resolution ranges from 15 to 60 m (Table 2-2). Seven of the nine bands are consistent with the Thematic Mapper (TM) and Enhanced Thematic Mapper Plus (ETM+) sensors found on earlier Landsat satellites, providing for compatibility with the historical Landsat data, while also improving measurement capabilities. Two new spectral bands, a deep blue coastal / aerosol band and a shortwave-infrared cirrus band will be collected, allowing scientists to measure water quality and improve detection of high, thin clouds. Acquired TIRS data will be registered to OLI data to create radiometrically, geometrically, and terrain-corrected 12-bit Landsat 8 data products. Note: the TIRS only has a three-year design life. The revisiting time of Landsat 8 is 16 days. Archived Landsat satellite images are best available at the USGS 'EarthExplorer' website (http://earthexplorer.usgs.gov/).

Table 2-2: Landsat 8 sensors bands, spectral and spatial resolution.

Spectral band OLI	**Wavelength**	**Spatial resolution**
Band 1 – Coastal / Aerosol	0.433 - 0.453 µm	30 m
Band 2 – Blue	0.450 - 0.515 µm	30 m
Band 3 – Green	0.525 - 0.600 µm	30 m
Band 4 – Red	0.630 - 0.680 µm	30 m
Band 5 – Near Infrared	0.845 - 0.885 µm	30 m
Band 6 – Short Wavelength Infrared	1.560 - 1.660 µm	30 m
Band 7 – Short Wavelength Infrared	2.100 - 2.300 µm	30 m
Band 8 – Panchromatic	0.500 - 0.680 µm	15 m
Band 9 – Cirrus	1.360 - 1.390 µm	30 m
Spectral band TIRS	**Wavelength**	**Spatial resolution**
Band 10 – Long Wavelength Infrared	10.30 - 11.30 µm	100 m
Band 11 – Long Wavelength Infrared	11.50 - 12.50 µm	100 m

ASTER

The Advanced Spaceborne Thermal Emission and Reflection Radiometer (ASTER) is an imaging sensor onboard of the Terra platform, which was launched in December 1999. ASTER, designed for scientific purposes, records data to create detailed maps of land surface temperature, reflectance, and elevation. ASTER provides high-resolution images of the planet Earth in 14 different bands of the electromagnetic spectrum, ranging from visible to thermal infrared light. The resolution of images ranges between 15 to 90 meters. Detailed description is provided in Table 2-3. Note: ASTER SWIR data acquired since April 2008 are not useable, and show saturation of values and severe striping. ASTER is an on-demand instrument, what means that data will only be acquired over a location if a request has been submitted to observe that area. Any data that ASTER has already acquired are available to all by ordering those data from the Earth Observing System Data Gateway (EDG). How to acquire ASTER data is described at http://asterweb.jpl.nasa.gov/gettingdata/; ASTER image data search via http://gds.ersdac.jspacesystems.or.jp/?lang=en. Commercial purchasing is possible via different reseller's, e.g. in Europe via e-geos (http://www.e-geos.it/products/pdf/prices.pdf).

Table 2-3. ASTER bands, spectral and spatial resolution.

Spectral Band	Wavelength	Spatial resolution	Nadir or Backward looking	Bit depth
Visible and near infrared spectrum				
Band 1 – Green	0.520 – 0.600 µm	15 m	Nadir	8 bit
Band 2 – Blue	0.630 – 0.690 µm		Nadir	
Band 3N – Red	0.760 – 0.860 µm		Nadir	
Band 3B – Red	0.760 – 0.860 µm		Backward	
Short-wave infrared spectrum				
Band 4	1.600 – 1.700 µm	30 m	Nadir	8 bit
Band 5	2.145 – 2.185 µm		Nadir	
Band 6	2.185 – 2.225 µm		Nadir	
Band 7	2.235 – 2.285 µm		Nadir	
Band 8	2.295 – 2.365 µm		Nadir	
Band 9	2.360 – 2.430 µm		Nadir	
Long-wave infrared or thermal infrared spectrum				
Band 10	8.125 – 8.475 µm	90 m	Nadir	12 bit
Band 11	8.475 – 8.825 µm		Nadir	
Band 12	8.925 – 9.275 µm		Nadir	
Band 13	10.250 – 10.950 µm		Nadir	
Band 14	10.950 – 11.650 µm		Nadir	

Sentinel-2 (planned Launch: April, 2015) will provide high-resolution optical imaging for land services. The Sentinel-2 mission will offer multi-spectral data with 13 bands in the visible, near infra-red and short wave infra-red part of the spectrum (cf. Table 4) 12 bit radiometric resolution, a high revisit (every 5 days at equator) under the same viewing conditions, high spatial resolution (10 m, 20 m and 60 m) and a wide field of view (290 km). Frequent revisits and high mission availability require two identical Sentinel-2 satellites operating simultaneously, which dictates a small, cost-effective and low-risk satellite. Compare the spectral and spatial resolution of Landsat 8 OLI, SPOT-6/7 and Sentinel-2 in Figure 2-1.

Table 4: Sentinel-2 spectral bands, wavelengths and spatial resolution.

Spectral Band	Wavelength (Center)	Spatial resolution	Spectral range
Band 1 – Coastal / Aerosol	0.443 µm	60 m	VIS
Band 2 – Blue	0.490 µm	10 m	
Band 3 – Green	0.560 µm	10 m	
Band 4 – Red	0.665 µm	10 m	

Band 5 – Red Edge	0.705 µm	20 m	NIR
Band 6 – Red Edge	0.740 µm	20 m	
Band 7 – Red Edge	0.783 µm	20 m	
Band 8a – Red Edge	0.865 µm	20 m	
Band 8 – NIR	0.842 µm	10 m	
Band 9 – Water vapour	0.945 µm	60 m	
Band 10 – Cirrus	1.375 µm	60 m	SWIR
Band 11 – Snow / ice / cloud discrimination	1.610 µm	20 m	
Band 12 – Snow / ice / cloud discrimination	2.190 µm	20 m	

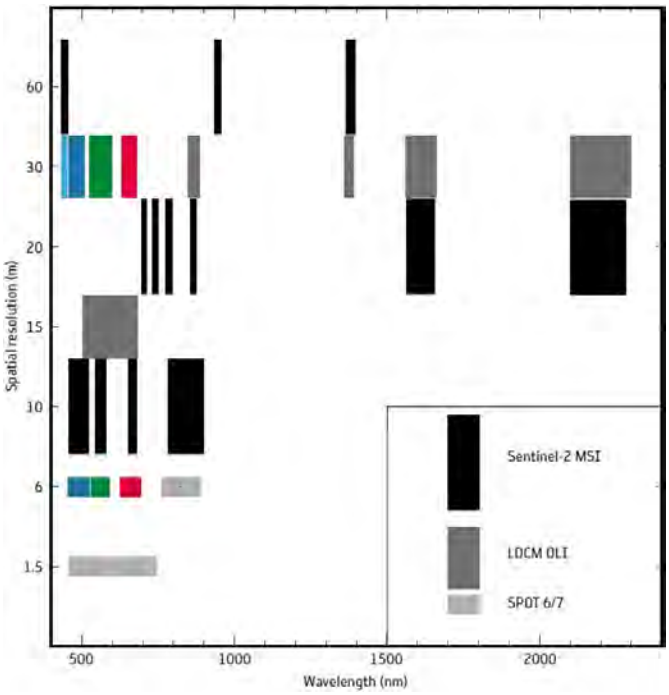

Figure 2-2-1: Comparison of spectral and spatial resolution of satellite sensors Sentinel-2, Landsat 8 OLI and SPOT-6/7 (adapted from Fletcher (2012)).

2.2.4 DIGITAL ELEVATION MODELS

Digital elevation models (DEM), including digital terrain models (DTM) and digital surface models (DSM), are an important source and more or the less standardized information for getting hints on hydrological and geomorphological conditions. In general DEMs differ in their production, either by active sensors (radar, LiDAR) or passive optical sensors and therefore are different in resolution, as well vertical and horizontal accuracy. The most

prominent global, available for free and consistent DEMs are SRTM (radar) and ASTER GDEM (optical); more accurate global DEMs will be available soon. Whereas both are available in enhanced post-processing versions, ALOS data (optical: panchromatic) is another reasonable option with higher DEM spatial resolution (ca. 10 m), but has to be processed for individual tasks. Pricey solutions coming along with up to very high resolution DEMs (1 to 5 m), which requires individual tasking, can be calculated from stereo satellite imagery using satellite sensors such GeoEye-1, WorldView-1, WorldView-2, IKONOS, Pleiades-1, SPOT-5, SPOT-6 and SPOT-7 satellite sensors.

The Shuttle Radar Topography Mission (**SRTM**), conducted in 2000, obtained radar data by sensors (*Spaceborne Imaging Radar-C/X-band Synthetic Aperture Radar* (SIR-C/X-SAR)) mounted on the Space Shuttle Endeavour with the purpose to generate digital elevation models on a near-global scale from 56° S to 60° N. The resolution of SRTM data ranges from 1 arcsecond (ca. 30 m), over 3 arcsecond (ca. 90 m) to 30 arcseconds (ca. 1 km). Since the original SRTM data contains voids, especially in terrain with high relief, several efforts were conducted to fill the voids and to enhance the topographical data. The 3 arcsecond SRTM is globally available in the latest version 4 and was calculated by CGIAR (http://srtm.csi.cgiar.org/SELECTION/inputCoord.asp), as well as the LP DAAC released the NASA Shuttle Radar Topography Mission (SRTM) Version 3.0 (SRTM Plus) Product collection with all voids eliminated, where these were filled primarily with ASTER GDEM2 data. Recently, the 1 arcsecond SRTM has also been made available globally.

The **ASTER GDEM product**, derived from ASTER satellite imagery (see above), is available at 30 m spatial resolution and downloadable for free e.g. via the web-platform: http://reverb.echo.nasa.gov/reverb/. In its 2nd version improvements include increased horizontal and vertical accuracy, better horizontal resolution, reduced presence of artefacts, and more realistic values over water bodies. Nonetheless, ASTER GDEM is derived from optical data, it is not necessarily be of better quality than SRTM 3 arcsecond data and has to be used with care.

SRTM-X data with a spatial resolution between 25m and 30m are available for free for certain flight paths. However, none of the declared study sites lie within the covered areas. While the total land coverage at high latitudes is almost 100%, it is very thin around the equator. The test sites Nuba Mountains (South Sudan; Tile E020N10) and Gambella (Ethiopia; Tile E030N00) partially lie in the covered areas. They can be downloaded for free after registration at DLR EOWEB. An overview for the total covered area of this mission can be found online[1]. No further missions are planned at the moment.

TanDEM-X data can be purchased at different product levels and charges for accepted proposals at DLR EOWEB. Spatial resolutions of 12 m (standard product) 30 m and 90 m are available, however they vary in their absolute vertical accuracy (< 10m, <18m, <30m). The swath width is about 30x50 km:

[1] http://geo.ebp.ch/downloads/SRTM%20X-SAR%2025m.kmz

CoSSC Data Proposal: Bistatic image acquisitions for proposed areas. The delivery product is the Co-Registered Single Look Slant Range Complex (CoSSC) product, which is an interferometric pre-product of the TanDEM-X processing chain. Generating DEMs requires various user decisions and manual inputs so no automated DEM generation is possible. Costs: 100 € per product (COFUR price list: Cost Of Fulfilling User Request)

DEM Data Proposal: TanDEM-X Digital Elevation (DEM) products, which are announced via Proposal Call. The delivery product contains the DEM as a Geotiff raster image. Costs: None given.

Purchasing TanDEM-X products (12m spatial resolution, 30 km swath) directly from the EOWEB portal costs 800 - 1300 €. Astrium GmbH also sells TerraSAR-X and WorldDEM products[2].

TerraSAR-X products (granted by the DLR proposal) can be processed to a DEM if two acquisitions are made within a short time period. They need to be ordered as SSC products with phase information (Proposal LAN025). However, as TerraSAR-X is a German satellite and many of the study areas lie in conflict areas, the delivery of the products has to be approved by the German Federal Office for Economic Affairs and Export Control / Bundesamt für Wirtschaft und Ausfuhrkontrolle (BAFA), costing 50 € per application (via DLR) and consuming additional 4-12 weeks before delivery. At least, no application was denied by the BAFA so far, which means that all ordered datasets have been delivered. Currently image pairs of Dagahaley, Kenya and Kalemie, DRC from 2014 have been ordered to test the feasibility of this approach. Based on experiences with previous orders they are expected to be delivered in late 2014. The dataset of Kenya is supposed to arrive earlier as it is not part of the "negative list" with determines the countries of which images need to be applied for.

Sentinel-1 was launched in April 2014 and is operational since October 2014 (https://sentinel.esa.int/web/sentinel/home). First images are supposed to be delivered in spring 2015, but European regions are prioritized in the first phase. They have a spatial resolution of 5 meters and will be delivered at no cost. Although the DEM generation out of Sentinel-1 data has not been investigated yet, it should theoretically work similar as for other sensors (e.g. TerraSAR-X). Sentinel-1 could be a valuable source for EO4HumEn, however many points are unclear at present so it is more an alternative than an indispensable source.

Sentinel-1 data will be available via the Sentinel Data Hub portal[3]. Only a free registration is needed to search and download tiles. However, due to the high spatial resolutions the data volume of both raw and processed data and the needed memory are expected to reach new dimensions.

[2] http://www.astrium-geo.com/en/122-price-lists

[3] https://senthub.esa.int/

2.3 MAPPING METHODS

2.3.1 LITHOLOGY

The potential of optical remote sensing data for geological mapping has long been appreciated by the scientific community. The methods to derive lithology from multispectral RS data are described in standard textbooks such as Gupta (1991), from which most of the following description is abstracted. It has to be kept in mind that the spectral response recorded over a rock unit by a multispectral sensor such as Landsat 8 or its predecessors is a function of several factors, including the rock type, the state of weathering, moisture content, soil cover and vegetation, which are interdependent. Spectral responses can vary largely between fresh and weathered rock. Therefore, the spectral properties recorded in multispectral data are usually not sufficient to identify specific rock types without any ground truth data from the field. Multiple converging evidence from the general geologic setting, the type of landform, the weathering style, the drainage system and the vegetation cover developed in the investigated unit can under favorable conditions allow a distinction of major rock types, but an image derived geological map remains an interpretation, before it has been validated by fieldwork (Prost (2002), p. 169). Thus, the aim of remote sensing data interpretation can in many cases be merely to *distinguish* different rock types in the study area rather than *identifying* them, which still greatly reduces the amount of fieldwork compared to traditional geological mapping. That said, a number of techniques have been developed to emphasize spectral differences between different rock units to aid geological interpretation, in conjunction with textural and structural clues. These techniques often require the image analyst to select and fine-tune the preprocessing of the data on a trial-and-error basis to make faint differences between rock types more apparent.

2.3.1.1 Band combinations

The simplest way to explore multispectral imagery like Landsat data is to use false color composites of different sensor bands. In this way, relative variations in the intensity levels between the bands become apparent, highlighting the spectral differences between the surface units. This method profits from the fact that the human vision can distinguish different colors much better than variations in grey level, for example when each channel is analyzed individually or the bands are observed side by side rather than as an RGB false color composite. Which band combinations are best to be used depends on the image content and has to be determined by visual inspection and trial and error. In many regions, the different color bands are highly correlated. Therefore, it makes sense to use the bands that have the least correlation. This can be calculated by most remote sensing software packages. Another reasonable approach is to avoid the blue and green channels due to atmospheric effects, that are strongest in this region, and to use red, near infrared, and short wave infrared in combination, as vegetation reflects strongly in the near infrared (NIR), and certain rock types have absorption features in the short wave infrared (SWIR), leading to stronger variations in greylevel in that channel compared to other bands. To obtain the best results for visual interpretation, each band should be stretched to their actual dynamic range, and the

frequency histograms of the three bands should be made similar to each other (histogram stretching). The bands can also be displayed in the intensity-hue-saturation color system, which might lead to more apparent color variations between rock units.

2.3.1.2 Band ratios

The main effect of rationing image bands against each other by division of their respective DN values is the suppression of shade and shadow effects, which are at first order linear over the wavelengths, and therefore the same in the two bands. Therefore, subtle spectral differences become more apparent. The choice, which band ratios to use is again in part subjective, and involves comparison of the results with outcrops of known rock types. However, certain combinations have been proven useful to distinguish different rock types based on their spectral properties. They are shown in table 3 above. It has to be kept in mind that these methods only work if the rock surface is not covered by vegetation, regolith or burned areas. Of course, the output of these ratios can be input to color composite images.

Table 3: Important band ratios for surface compositional discrimination[4]

Landsat 7 (ETM+)	Landsat 8 (OLI)	Application
7/5	7/6 (SWIR2/SWIR1)	Argillic vs. non-argillic
3/4	4/5 (NIR/Red)	Rocks vs. vegetation
5/1	6/2 (SWIR1/Blue)	Iron-bearing vs. iron-free
5/4	6/5 (SWIR1/NIR)	Argillic vs. Fe^{2+}
4/7	5/7 (NIR/SWIR2)	Argillic vs. Fe^{3+}
4/2	5/3 (Red/Blue)	Fe^{2+} vs. Fe^{3+}

2.3.1.3 Principal component analysis

Another useful technique to make spectral differences between surface units more apparent is the principal component analysis (PCA). It is basically a transformation of the coordinate system of the feature space. The new coordinate system of the feature space is calculated in such a way that the first axis is oriented in the direction of the maximum variance contained in the input data. This usually corresponds to overall variations in brightness due to shadow effects. Once this first axis has been defined (named PC 1), the next principal component is calculated

[4] Modified after Drury and Hunt, 1989, Geological uses of remotely sensed reflected and emitted data of laterized Archean terrain in Western Australia. Int. J. Remote Sens. 10(3): 475-497

along the largest variance perpendicular to the first principal component, and so on. The result is a multiband dataset with the same number of bands as the input data, where most of the information is contained in the first few bands, whereas the latter bands contain mostly noise. After visual inspection, these noise-dominated bands can be discarded, reducing the number of bands to be analyzed. More importantly, as the principal components are non-correlated, an RGB-display of three PC bands shows surface units with different spectral properties in vivid colors, making a distinction of units easier. As the PCA result is dependent on the content of the image investigated, the result of PCA looks different if the input image subset is changed. Likewise, outcrops of the same rock type in neighboring images will be displayed differently in the PC results of the two images. Therefore, PCA can be helpful to discriminate surface units from each other, but ia not suited for an actual identification of rock types. To this end either outcrops with known composition have be present, or the untransformed spectra of the units previously identified with PCA have to be analyzed thoroughly for spectral clues, possibly using band ratios.

2.3.1.4 Clues to identify different lithologies

As stated above, the mapping and identification of different surface units usually depends on converging evidence from the spectral response, the textural properties, the identification of typical landforms, and context information. The following section briefly introduces typical features of different rock types or classes of rocks. It has been abstracted from Gupta (1991).

Sedimentary rocks

The most prominent feature of sedimentary rocks is the compositional layering of rock types often possessing different physical properties, which can result in different spectral properties, resistance to erosion, variations in moisture content or banded vegetation. This frequently results in banding observed in remote sensing imagery, which tends to be longer and more regular than banding produced by foliated metamorphic rocks.

Sandstones are generally resistant to weathering, and therefore tend to form topographically prominent landforms such as hills, ridges, mesas and cliffs. The rocks develop a medium to low density drainage system due to the generally good permeability. Jointing is well developed, often leading to a rectangular or angulate drainage pattern. Sandstone generally supports good vegetation cover due to good porosity and permeability. It appears light-toned in VIS-NIR-SWIR imagery. Especially in arid regions, they can appear similar to limestones, but lack their characteristic absorption feature at 2.35 µm (SWIR). Also, quarzites appear similar, but occur in metamorphic environments.

Shales are generally easily eroded, and therefore tend to form low grounds and valleys. Gently rounded hills can be found in humid climates. The generally impervious nature of these rocks results in a well-developed, fine-textured, dense drainage system. Prominent jointing or bedding is rarely observed. Shales can produce a thick soil cover in humid climates. In arid to semi-arid climates, vegetation is sparse or nearly absent, in humid climates, vegetation bandings may mark the lithology; here, shales are also often used for agriculture. Shales appear light-

toned in VIS-NIR-SWIR images except in the 2.1-2.4 µm region, where clay minerals possess absorption features. Other soft sedimentary rocks like schists and phyllites appear similar in remote sensing imagery, but differ in their regional setting.

Carbonate rocks like limestones and dolomites are generally resistant to erosion in arid climates, forming ridges and hills. In humid climates, they display typical features of karst topography: collapse structures, sinkholes, caverns, trenches, disappearance of surface streams. Jointing is generally well developed and often accentuated by karst features. The drainage density is generally low. The soil on top of carbonates is often light-colored or reddish due to residuals of the solution process. Carbonates are generally light-toned in VIS-NIR-SWIR images except around 2.35 µm; iron-bearing weathering residuals can lead to absorptions in the UV-blue region. SAR data may help to detect characteristic karst features, as it penetrates the often dense vegetation cover. Carbonate rocks can be confused with sandstones, if no clear karst features are observed or the spectral resolution allows the identification of the 2.35-µm-absorption of limestones.

Igneous rocks

The main characteristic feature of igneous rocks is the absence of bedding or foliation. Intrusive igneous rocks are massive, isotropic and homogeneous over large areas, and often well jointed. The drainage is dendritic or angular. These rocks occur in different shapes and dimensions, from batholiths to dykes and sills. Extrusive igneous rocks can be identified by their associated volcanic landforms: volcanic edifices, lavaflows, cones, craters and the like. The flows have a rough surface topography and discordant contacts with the underlying rock. Sets of lava flows can give the impression of rough sub-horizontal bedding. Extrusive rocks can be very susceptible to weathering, making the identification of older units difficult due to soil and vegetation cover.

Granites occur as large intrusive bodies. They show a great variety of weathering characteristics. In warm humid climates, they typically exhibit spheroidal weathering with smooth, rounded shapes; the topography is low-lying, sometimes woolsack weathering is observed. In arid and semi-arid regions, but sometimes also in the tropics, steep, sharp and jagged forms develop. The drainage density is usually low to medium with angulate patterns due to the often prominent jointing. Granites are usually light toned in the spectral regions of reflected sunlight, but the spectral response can vary significantly according to composition, weathering state and soil/vegetation cover.

Mafic intrusive bodies are usually darker but have a similar appearance in remote sensing imagery and may be confused with granites. They are highly susceptible to weathering and alteration, especially under humid conditions. The presence of iron-rich minerals (pyroxenes, biotite, amphibolites) lead to dark tones, especially in the blue region. Alteration products can comprise clay minerals with absorption bands between 2.1 and 2.4µm. A vegetation cover on ultramafic rocks can be absent due to the toxic effects of certain metals contained in them. Dolerites are intrusive mafic rocks, which form horizontal sills, which are difficult to distinguish from layered (sedimentary) host rocks, if no discordant contacts are observed, and vertical dykes, which often stand out above the surrounding country rocks, forming walls.

Acidic extrusive rocks are easily eroded, older flows are therefore difficult to identify. They are highly porous, leading to a very coarse or absent drainage pattern. The general appearance features an oblate outline, rough topography and a hummocky surface. Basaltic lavas have a lower viscosity than acidic lavas, resulting in flatter, ropy textures. They can display typical columnar jointing. The most prominent evidence for these rocks are flow structures and associated volcanic landforms. Differences in surface roughness observed in SAR data may help distinguish lava flows of different ages.

Metamorphic rocks

Metamorphic rocks are marked by foliation and faint stratification. The foliation is observed as curvilinear, sub-parallel lineaments in remote sensing data. They are generally similar to their non-metamorphic derivatives.

Quartzites are generally resistant to weathering in humid and dry climates, and therefore form hills, ridges and scarps. Rectangular and angulate drainage patterns are common due to very prominent jointing. Their general appearance is similar to sandstones, but they occur in a metamorphic setting.

In dry climates, marbles are relatively resistant to erosion, and therefore form cliffs, hills and ridges similar to quartizes and sandstones. Under humid conditions, they show karst features, which can also result in a low drainage density. Marbles can display a highly deformed foliation due to plastic deformation. Joints are often well developed. Like limestones, these rocks exhibit an absorption band at 2.35 µm and are otherwise light-toned.

Schists and phyllites, the metamorphosed counterparts of shales, are generally incompetent rocks, occurring in valleys and lower hill slopes. They often display a well-developed, dense, dendritic drainage pattern, sometimes controlled by a strongly developed foliation. As for shales, the vegetation cover is sparse in arid and semiarid conditions, and fairly dense in humid climates. The spectral characteristics vary with their mineral content, but in general, iron-rich minerals result in dark tones in the blue band. Clay-rich weathering products lead to strong absorption at 2.1-2.4 µm.

Gneisses generally form low-lying, undulated terrain in a metamorphic setting, characterized by foliated and banded relief caused by intercalation with other rock types. They can cover large areas. The spectral features vary greatly, depending on their composition. Jointing is well developed. Gneisses appear similar to acidic intrusive rocks, but may be distinguished by the presence of foliation and banded relief. They can also be similar to schists and phyllites, but typically have a coarser foliation.

2.3.2 STRUCTURAL GEOLOGY

2.3.2.1 Layering and folding

Structural geology encompasses the three-dimensional distribution of rock and sediment bodies, and the presence and orientation of deformational structures such as folds, faults and fractures/joints. Understanding the structural geology of a study area is important to describe the probable continuation of aquifers and aquicludes into the

subsurface, and to assess, which structures observed in the image might represent open fissures that are possible pathways for groundwater.

The orientation of sedimentary rock layers is described by their strike and dip, and is important to project the depth at which a given aquifer might be encountered when drilling at a given location. Qualitative statements about the strike and dip can be made relatively straight forward, provided that layer boundaries are well visible in the image. Draping the image or the photogeological map over a DEM for 3D display can be very helpful to understand the orientation of rock units, which is not always easy using only the map perspective. A very handy tool to this purpose is Google Earth, as it allows 3D visualization without any further effort. Quantitative measurements of strike and dip can be made if the elevation and position of at least three points on the surface of the same rock layer can be measured from a DEM. In this case, a plane can be fitted to these three or more points, giving the estimated strike and dip of the layer at this location. A useful tool for these measurements is the Layer tool plugin for ArcGIS, provided by Kneissl, van Gasselt and Neukum (2010). With this tool, the user just clicks on the three or more outcrop points on a surface, and the tool calculates the corresponding plane and places the correct map symbol.

Folds can be delineated by tracing the bedding or marker horizon along the swinging strike, the doubling of layer sequences, and the recognition of the dip direction. Therefore, open longitudinal folds are easy to recognize in satellite images. Very tight folds can be difficult to recognize, because of the smaller areal extent of hinge areas. In maps, folds are marked with the symbols for synclines and anticlines, respectively. The recognition of folds is important to understand the general structural geology of the study area, but they are also relevant for the groundwater flow by themselves, as the bending of sedimentary layers can lead to open joints along the hinges, which are potential water pathways.

2.3.2.2 Lineaments

As introduced in chapter 1, structures that are observed as lineaments can act as barriers or as conduits for groundwater flow. Therefore, their mapping is an important step in areas characterized by sedimentary or crystalline rocks. Lineaments can be mapped using satellite imagery, DEMs or Radar data. All three datasets and corresponding methods have their advantages and disadvantages. In the next section, practical aspects of lineament mapping using different datasets will be explained.

Lineaments from optical data

Currently, the most commonly used satellite imagery is Landsat 8 with high resolution data and at no costs. Pansharpening of Landsat 8 results in spatial resolutions up to 15 m and is sufficient in most of the studies applied. Other data with higher spatial resolution may be an option for areas with complex geological conditions; a list of satellite sensors is given in section 2.2.3. Filtering of the image data with edge-enhancing filters like the *Sobel operator* or the *Canny filter* or the reduction of data redundancy with *principal component analysis* (PCA) can be

helpful to enhance the perceptibility or detectability of lineaments. Multi-band (> 3) / Multi-temporal combinations have shown the best results for delineating lineaments. Multi-band infrared in combination with DEM curvature highlight the 2.5D impression of earth surface and multi-temporal data reveal temporal artefacts e.g. burned areas. The automated extraction of lineaments is offered by different software products like Geomatica software, Orfeo – Monteverdi, or Trimble eCognition. However, manual overwork on automatically derived lineaments is essential.

The main drawback of optical image analysis that illumination differences in rough terrain due to shadow can lead to large spectral differences, which may render lineaments at a certain orientation difficult to recognize. Additionally a best suited satellite image (almost no clouds, in optimal season: dry is advantageous) has to be requested, which is often time consuming, and avoided when only DEM data is used.

Lineaments from DEMs

Deriving lineaments from DEMs is advantageous to optical data, since height information is a somehow a standardized information and therefore developed methods can be easily transferred to different study areas. DTMs should be favored to DSMs as these reflect better the undulation of the earth surface and do not include unwanted elevation information, such as e.g. vegetation height. To delineate lineaments from DEMs first order (slope, aspect) or second order (profile curvature, plan curvature) derivatives can be calculated. The calculation of the overall curvature, including both profile curvature and plan curvature, has shown to be most practicable. Diverse filtering with moving windows of different size and calculating the mean or median may necessary if the elevation data includes unwanted artefacts (e.g. for ASTER GDEM) or too much detail. In general, median filtering will preserve contours and mean filtering will smooth the DEM. However, choosing the right moving window size depends on the roughness and complexity of an area. In most cases the spatial resolution of 30 m is sufficient for lineament extraction and advantageous to e.g. SRTM 3 arcsecond (ca. 90 m). In future SRTM with 1 arcsecond and available on global scale will be the data of choice.

Lineaments from Radar data

Due to the side-looking geometry of a SAR system and therefore, the low incidence angle of the Radar wave with respect to the Earth's surface can reveal subtle structures, which are not visible in the planar view of optical satellite imagery. Edge detection algorithms can then be applied to radar images of suitable spatial resolution in order to extract lineaments or junctions. However, as changes in surface roughness or moisture also produce changes in the radar backscatter the extracted edges have to be evaluated according to their likelihood being geologically relevant. Therefore all edge-pixels are converted to lines so their shapes and composition can be analyzed visually. Important variables are length, frequency, direction, drainage density and intersections. Topographic properties such as slope and aspect can also help to distinguish geological borders from surface characteristic changes.

How many and which edges are detected strongly depends on the flight direction of the sensor. Features lying parallel to the flight direction are more likely to be detected. Multiple passes (ascending and descending) can be combined in order to get a more complete result. However, as both ascending and descending orbits are moving from the poles towards the equator, structures of latitudinal orientation (± 20°) can still be "overseen" or at least found to a lesser degree.

The spatial resolution of Level 1.1 SSC TerraSAR-X products is about 1.7 meter. A conservative preprocessing (less multiple looks and large scaled adaptive speckle filtering) can result in data resolutions smaller than 10 meters. This is estimated to be sufficient for the mapping of geologic features.

Once a suitable algorithm is found, ordering is the main constraint regarding a quick provision of usable products. By now, it took up to 115 days from the ordering of a scene to the delivery. New data can be acquired within 11 day repeat cycles. Because commercial orders of TerraSAR-X products are processed with a higher priority, a tolerance of ± 2 repeat cycles is advised, resulting in a total timespan of 44 days.

2.3.3 HYDROLOGY

Mapping of ephemeral and permanent surface water bodies is important to understand the general flow of groundwater and to identify recharge and discharge zones. The easiest, but possibly most tedious way is mapping of these features from optical imagery by hand. Especially abandoned river beds and ancient oxbows can reveal themselves by characteristic curved topographical patterns or variations in vegetation density. These features are important hints to grain-size distribution variations in areas of unconsolidated sediments, and can point to preferred groundwater pathways. Spring lines may also be revealed by aligned starting points of rivers or the sudden appearance of vegetation along a more or less straight line. Pixel- or object-based classification approaches may also be employed to extract the drainage system or parts of it, depending on the complexity of the scene. Finally, the drainage system can be extracted from a DEM of sufficient quality.

2.3.3.1 Drainage calculation from DEM

The drainage system can be extracted from a DEM relatively easily. This procedure has been applied in some of the test sites introduced in chapter 3 of this protocol. The success of this method depends on the quality and resolution of the underlying DEM. Therefore, results over flat terrain are less convincing due to noise in the datasets used here (SRTM, ASTER DEM), and the drainage network has to be extracted visually/manually. In areas with a higher relief, this procedure works well. It can be performed, for example in ArcGIS, using the Spatial Analyst Tools, and comprises the following steps:

1. Cells within the DEM that have no outflow are filled. This assures that no singular local sinks occur due to errors in the data (Spatial Analyst Tools>Hydrology>Fill).
2. For each cell, the flow direction with respect to its eight neighbors is calculated (Spatial Analyst Tools>Hydrology>Flow direction).

3. Now, the upstream area for each cell is calculated (Spatial Analyst Tools>Hydrology>Flow accumulation).
4. All cells with a contributing drainage area larger than a user defined threshold are selected. The choice of the threshold depends on the quality of the underlying DEM. In ArcGIS, the Raster calculator can be used for this operation: Con("Flow Accumulation" >1000,1) marks all cells that have a catchment (=flow accumulation value from step 3) bigger than 1000 cells with 1, all other cells with 0. This step extracts the flow network.
5. The resulting network can be divided into stream orders (Spatial Analyst Tools>Hydrology>Stream order).
6. Finally, the results can be converted to vector data (Spatial Analyst Tools>Hydrology> Stream to feature).

The right figure below shows the result of the extraction of a drainage system with ArcGIS, in the left figure a manual digitization based on Bing-Maps is shown. The results are quite similar but the difference is the required working time of the operator. Thus, this method is a good way to extract big drainage systems in a short time and to get an overview of surface structures and possible spring areas.

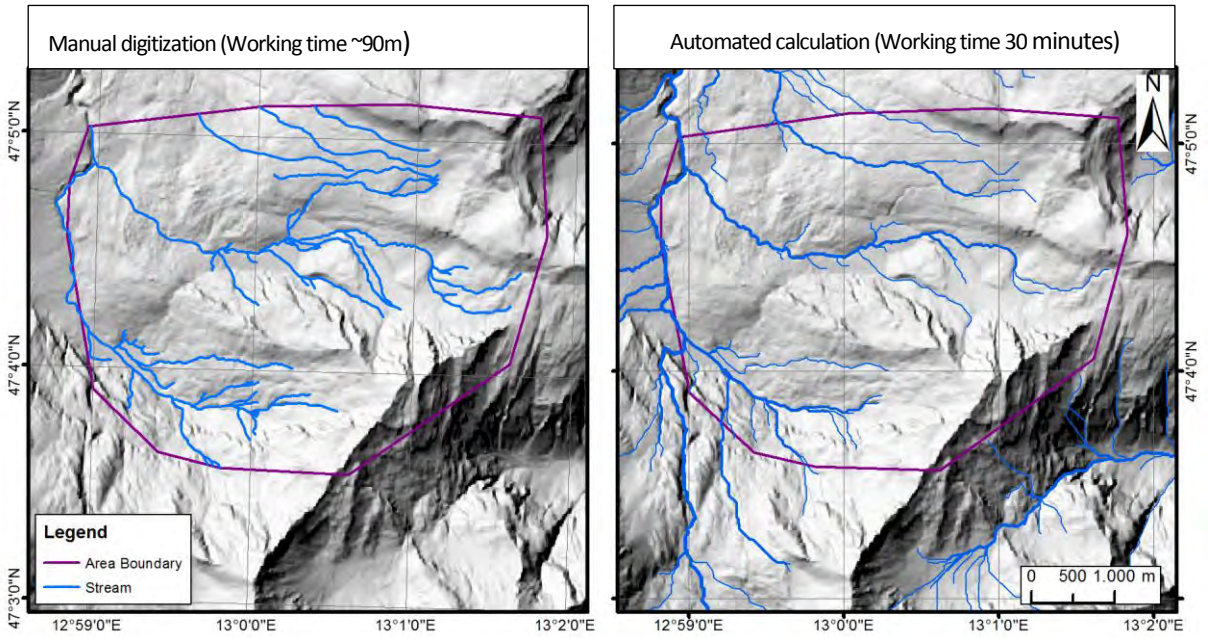

Figure 2-2: Manually digitized and automatically extracted drainage system at the Rauris testsite (see section 3.3)

2.3.3.1 Mapping of buried channels using SAR data

Under favorable conditions, abandoned paleochannels buried under a thin surface cover of loose sediments can be detected using radar data. These channels are usually more permeable than the surrounding material due to the sediments of larger grain size found here. The longer the wavelength, the deeper is the radar penetration, at the expense of spatial resolution. ALOS PALSAR is suitable for estimating sub-surface properties under certain

conditions. Within this project, access to 50 ALOS PALSAR products from the archive is granted by proposal 21171 by Uni Tübingen. Archive data reaches from 2009 to 2011. Data can be searched and ordered via the EOLiSA-software[5] and is provided at no costs within a week by ESA/JAXA. The spatial resolution depends on the product (Fine Mode [swath 40km], ScanSAR [swath 250km], polarimetric). But for single polarizations resolutions up to 7 m can be achieved.

ALOS-2 has been launched in May 2014 and is expected to deliver images in 2015. As it is a continuity mission methods tested on ALOS-1 can be applied on the new data. However, no proposals can be submitted at the moment and no information about the prices is available.

The *optimum* conditions for sub-surface imaging with orbital radar in arid regions are:

1. Smooth surface of fine-grained and well-sorted sand
2. Very dry conditions (less than 1% moisture content) to minimize the effect of electrical conductivity on radar backscatter and to have greater signal ground penetration
3. Limited depth of sand cover (signal is attenuated at a depth of 2 meters when soil moisture is at 1%).
4. Sub-surface imaging occurs when a rough sand/bedrock interface produces strong backscattering (due to high roughness)
5. Further favoring conditions are look angles greater than 30° and cross-polarized bands (HH/VV, ALOS PALSAR Polarimetric Mode)

From the above conditions it is clear that this method only works under very dry surface conditions – under which it is questionable if the detected paleochannels will be water-bearing.

2.3.3.2 Soil moisture from radar data

Studies exist (Baghdadi, Aubert and Zribi (2012), Baghdadi et al. (2011), Kseneman, Gleich and Potočnik (2012)) which estimate soil moisture from TerraSAR-X data. However most of them are restrained to bare soil with only a thin herbaeceous layer (NDVI < 0.25). Typically, soil measurements are taken during the image acquisition time in order to correlate the radar backscatter with the measured values. However, collecting ground truth information is not possible in our case. This point is crucial as the backscattered signal not only responds to soil moisture but also to surface roughness and texture. Comparing two images acquired during rainy and dry season should help estimating the effect of moisture on radar backscatter. This approach at least gives information on relative moisture changes. Experimenting with these techniques is an ongoing work in the EO4HumEn project. Additionally, empirical equations correlating soil moisture and σ_0(db) Sigma Naught of TerraSAR-X of other studies in Africa are searched to get a rough understanding on soil moisture in our study areas.

[5] http://earth.esa.int/EOLi/EOLi.html

2.3.3.3 Possible contaminants and access restrictions

Possible groundwater pollutants should be included into the hydrogeological reconnaissance map. These might include villages, especially latrines, industrial installations, cattle grazing areas, and so forth. These features might be visible in very high resolution imagery that has been ordered specifically for this project or is otherwise available. Alternatively, Google Maps and Bing images should be considered. These data are not always up to date, but should nevertheless be checked.

Also, existing roads and recognizable obstacles for transportation of a drilling rig should be mapped. To this end, OpenStreetMap (OSM) can be a useful source, which can be included into ArcGIS as a non-editable external layer, or as an editable dataset using the ArcGIS Editor for OSM. Again, VHR imagery is useful to map these features.

2.4 FROM DATA ANALYSIS TO THE FINAL HYDROGEOLOGICAL MAP AND DRILLING SITES

To assess the hydrogeological situation of a study site an expert based evaluation of the above described geological and hydrological findings is necessary. Results from remote sensing investigations about lithology and structural geology can be used to identify and delineate water bearing structures or regions, respectively, based on a quantification of their permeability. However, as seen from figure 2-3 and table 4, this quantification is not straight forward, as the permeability of certain lithology can vary over several orders of magnitude, therefore, further information from the field- and laboratory work is often required for an accurate characterization of an area.

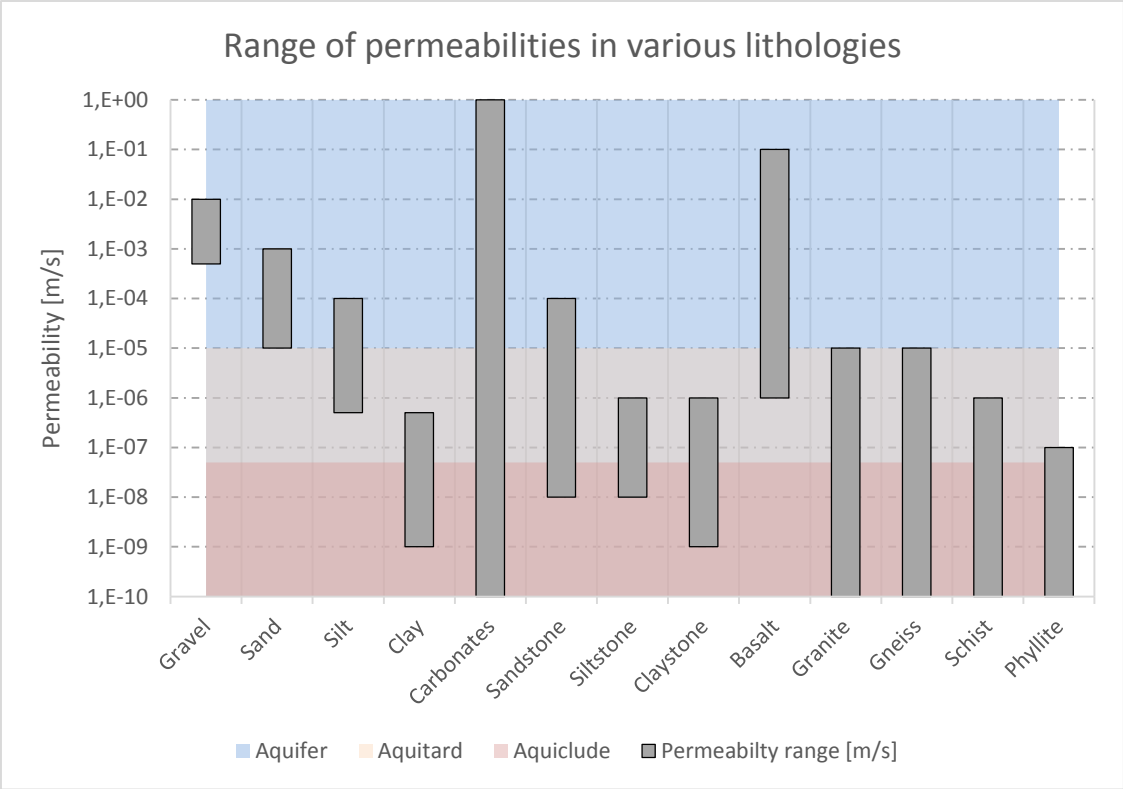

Figure 2-3: Range of permeabilities for various lithologies

Table 4: hydrogeological characteristics of different lithologies and structural settings (permeability data after Langguth and Voight (2004))

Aquifer Type	Lithology	Maximum effective permeability [m/s]	Minimum effective permeability [m/s]	Permeability determining factor
Porous aquifers in unconsolidated sediments	Gravel	10^{-1}	$5*10^{-4}$	Grain size distribution
	Sand	10^{-3}	10^{-5}	
	Silt	$5*10^{-4}$	$5*10^{-7}$	
	Clay	$5*10^{-6}$	10^{-9}	
Fractured hard rock aquifers (Sedimentary rocks)	Carbonatic rocks	10^{0}	10^{-10}	Fracture network and karstification
	Sandstone	10^{-4}	10^{-8}	Fracture network and matrix porosity
	Siltstone	10^{-6}	10^{-8}	
	Claystone	10^{-6}	10^{-9}	

Fractured hard rock aquifers (crystalline rocks)	Basalt	10^{-1}	10^{-6}	Fracture network and matrix porosity
	Granite	10^{-5}	10^{-10}	Fracture composition
	Gneiss	10^{-5}	10^{-10}	
	Schist	10^{-6}	10^{-10}	
	Phyllite	10^{-7}	$<10^{-10}$	

The permeability of porous aquifers in unconsolidated sediments is mainly controlled by their grain size distribution and can be easily estimated by characterizing the depositional processes (fluvial, lacustrine or eolian) in the region based on remote sensing (see chapter 1). As shown in figure 2-3, gravelly or sandy deposits (related to fluvial mass wasting) can be characterized as aquifers. Groundwater can be exploited anywhere in the range of these deposits. Main factors for the drilling site decisions are topography and surface runoff to determine the flow direction and knowledge about potential contaminants. To protect drinking water from contamination the potential borehole site must be located upstream of camps, settlements, factories, regions of intensive agricultural activities or further potential emitters of pollutants. In most cases it should be possible to identify the general direction of groundwater flow of a porous aquifer as well as potential contaminants by means of RS data. Hence, in the majority of cases sufficiently detailed hydrogeological maps and drilling sites can be delivered without further investigations in the field.

The wide range of possible permeabilities of fractured and karstifiable hard rock aquifers requires a detailed analysis of structures and their hydrogeological properties to decide whether a rock formation may act as aquifer ($K >= 10^{-5}$ m/s), as aquitard (10^{-5} m/s > K > $5*10^{-8}$ m/s) or as aquiclude ($K<5*10^{-8}$m/s). On the other hand, understanding the structural situation of a region does not automatically mean to understand their hydrogeological characteristics since brittle structures may act as flow paths or as barriers due to the lithology and the structure forming processes (see chapter 1). Besides hydrological input and the evaluation of possible contaminants an expert based hydrogeological assessment of each test side that incorporates auxiliary data such as geological maps or drilling logs is crucial to develop a complete and detailed hydrogeological map with all elements listed in table 2. As in the case of porous aquifers, the above mentioned general flow direction with respect to potential contaminants must be taken into account.

Based on a remote-sensing based hydrogeological reconnaissance map, the flow direction and knowledge about contaminants it is possible to delineate most suitable regions for drinking water exploitation. However, in many cases hydrogeological field work such as geophysical investigations or field mapping within the delineated area will finally be necessary to pinpoint a suitable drilling site in hard rock environments.

3 EXAMPLES FROM DIFFERENT LOCATIONS AND GEOLOGICAL SETTINGS

Dominating Geology	Arid climate	temperate climate	Tropical climate
Unconsolidated sediments	Not yet investigated	not yet investigated	Gambela, Ethiopia
Sedimentary rocks	Domeez, Iraq	Not yet investigated	not yet investigated
Crystalline rocks	Nuba Mountains, Sudan	Rauris, Austria	Paoua, CAR

Table 5: The test sites and their geological and climatic settings

We selected test sites located in unconsolidated sediments, sedimentary rocks and crystalline rocks to cover a wide range of geological situations. The test site Gambela stems from a request by MSF for the support of a refugee camp. This area is dominated by unconsolidated sediments, a fairly simple situation. No further investigation was required for the test sites in Yida and Jamam, which are characterized by similar geological settings.

The test site Domeez is very well suited to demonstrate the capabilities of remote sensing to distinguish lithology and to derive the geological structure in folded sedimentary deposits due to the very limited vegetation cover.

The Nuba Mountains have been selected as a site dominated by crystalline hard rock, where the mapping of lineaments is the most important step for the hydrogeological assessment. The geology and climate in the Nuba Mountains are expected to be similar to possible future study areas in hard rock terrain in Africa, making this area a valuable test site. This area will be used for automated lineament extraction in the upcoming tasks of the EO4HumEn project.

The Rauris area has been chosen, because hydrologic conditions of this area have been field mapped in detail, which allows the evaluation of results obtained by remote sensing. As a test site within the Central European Alps one would expect humid climate conditions. So it seems that this test site does not really fit the climatic classification as wet/dry seasonal change. However, due to usually dry fall conditions and snowfall in winter groundwater recharge is restricted to snowmelt in spring and rainfall in summer. Hence, from the hydrogeological point of view it is appropriate to classify the test site as is.

The town of Paoua, CAR, is situated in crystalline rocks under a tropical climate. Due to the deep weathering and dense vegetation cover, tropical areas are difficult to analyze by remote sensing. On the other hand, with respect to their hydrogeological characteristics deeply weathered hard rocks (sedimentary as well as crystalline) may be compared to unconsolidated sediments. The resulting groundwater bodies in such environments often show more the properties of porous than of fractured hard rock aquifers. Due to a steady positive water balance

(precipitation exceeds evaporation all over the year) a permanent groundwater recharge is assured and exploitation of drinking water is comparably easy. RS assistance is presumably not often required in such environments. However, to assess the possibilities and limits of the above described best practice guide it is planned to apply the methods to tropical test sites in further steps of the project. As a first test site the location of Kalemie in the DR Congo is designated as a representative for sedimentary hard rock environment.

3.1 GAMBELA

Overview

This study site is located in the Gambela People's Region of Ethiopia near the village of Itang. It was requested by MSF to support the supply of the refugee camp Kule, hosting refugees from nearby South Sudan, with groundwater. According to a hydrogeological map of Ethiopia at the national scale this area features a moderately to highly productive, porous aquifer.

Data

The following data were used for this study:

Geological Map of Ethiopia, 1973, 1:2.000.000, Geological Survey of Ethiopia

Hydrogeological Map of Ethiopia, 1988, 1:2.000.000, Ethiopian Institute of Geological Surveys

Landsat 8 image of 28. March 2014, image number LC81710542014087LGN00

Landsat 7 image of 04. June 2001, image number LE71710542001155SGS00

Landsat 4 image of 24. July 1990, image number LT41710541990205XXX03

Landsat 5 image of 25. August 1987, image number LT51710541987237XXX01

Landsat 5 image of image 06. August 1986 number LT51710541986218XXX03

SRTM digital elevation model N08_E034_3arc_v1, coordinates N08° E34°

Additionally, the freely available VHRS imagery in Bing Maps and Google were used.

Results

'Gambela' study area is located in a sedimentary plain, which received sediments from the Ethiopian Highlands further to the east and north-east. It is drained towards the west by the Baro River, which eventually dewaters into the White Nile. Several ephemeral rivers run from the north-east towards the Baro River. The nature of the sedimentary plain, being lacustrian or fluviatile, is hard to assess from remote sensing data, and is not described in the geological maps used here. Therefore, a prediction of the expected grain-size distribution in the subsurface is not possible. The area features several hills that rise up to 250 m above the surrounding plain. They are interpreted as hard rock outcrops of unknown composition, and are likely associated to the Precambrian crystalline rocks in the highlands further north-east.

We mapped the distribution of the sedimentary plain and the hard rock outcrops based on Landsat 8 imagery and the DEM. The Baro River and its flood plain were likewise mapped using Landsat imagery and DEM. Imagery from several points in time were visually assessed for variations in flooded area and changes in distribution of vegetation, but mapping based on the most recent Landsat 8 image in combination with the DEM proved most

affective to outline the area that appears to be regularly flooded by the Baro River, because we did not find a Landsat image that was taken during a flood event on the river, which then could have been used for directly mapping the flooded area.

The ephemeral drainage system north of the Baro River was extracted visually using patterns of aligned vegetation as clues. The available DEM does not have a quality sufficient to extract the drainage system automatically in this mostly flat area. The settlements and roads were partly imported from OpenStreetMap data, and partly digitized from the freely available VHRS imagery in Bing Maps and Google Maps.

Two areas were suggested for further geophysical testing or drilling. As this area is dominated by a porous aquifer, groundwater is expected to be available everywhere. To avoid contaminations from the villages and the refugee camp, both sites are located upstream from these settlements.

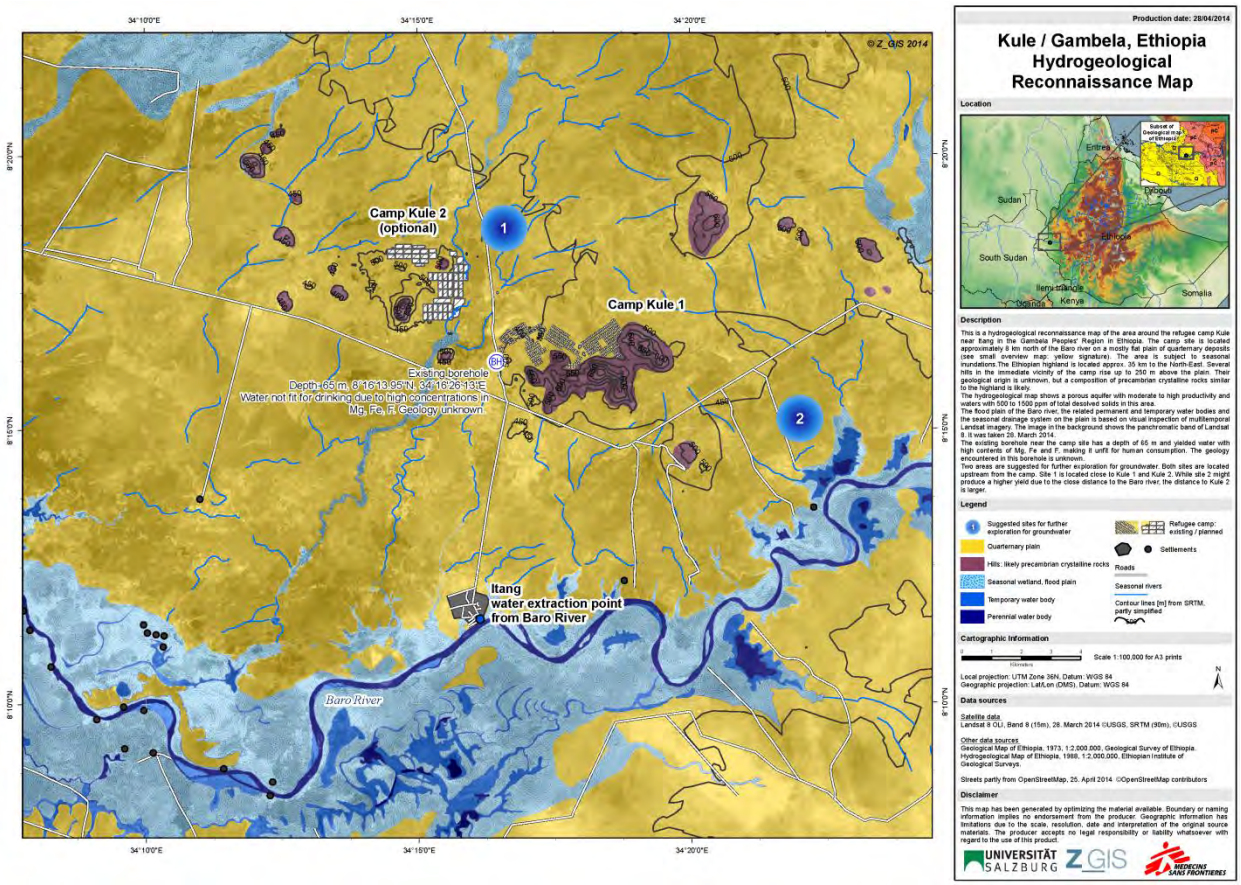

Figure 3-1: Hydrogeological reconnaissance map for the Gambela test-site

Conclusion

The hydrogeology in this test area appears to be relatively simple, and is dominated by a porous aquifer. As stated in chapter 1, the decision for potential drilling sites for drinking water supply under these conditions is mainly controlled by the regional and local flow direction with respect to potential pollutants. These two aspects have

been assessed by mapping the surface drainage system and the locations of the camp, villages and settlements, respectively. At the time of map production, only one borehole was known, and no information was available on the geology, depth to groundwater, and yield at this location. Therefore, gathering more information from local sources about this borehole, like further drilled wells possibly existing at large-scale farms in the area, and from existing hand-dug wells at the villages and settlements, would increase the knowledge about the distribution of sedimentary bodies in the subsurface. The water at the known drill site is reported to be high in magnesium, iron and fluorine. The high content of fluorine makes this water unfit for human consumption. The reason for this is unknown and can only be assessed by chemical analysis of water samples from different locations.

3.2 DOMEEZ

Overview

This test site is located in Iraq, 70 km north of Mosul (Figure 3-2). The study region covers an area of about 350 km² and the climate is semiarid. The surface elevation ranges from 300 m to 1300 m above sea level. The relief is dominated by a fold belt and overlying sediments. The site was suggested by MSF due to the refugee camp Domeez (near the city of Dahuk) hosting refugees from nearby Syria.

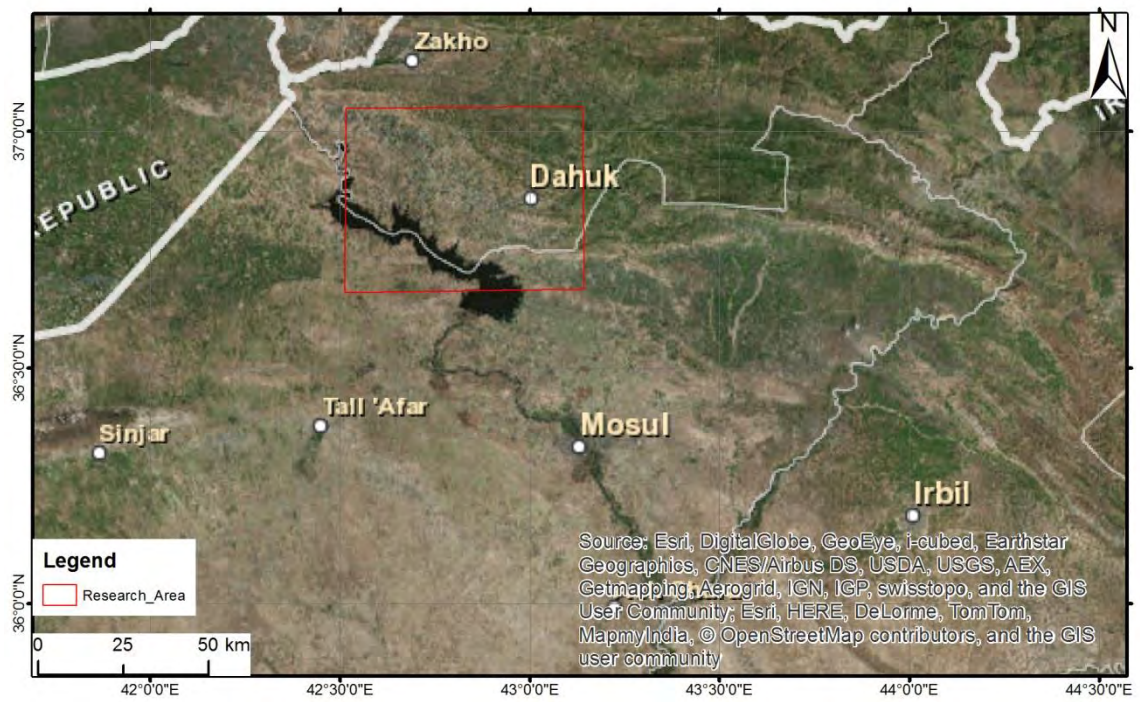

Figure 3-2: Overview map of Domeez testsite in northern Iraq

Data

The following data sets were used for remote sensing:

Landsat 8 image of 06. June 2013, image Number: LC81700342013157LGN00

DEM: SRTM 3 arcsecond, released 01. February 2005

SRTM3N36E042V1 Coordinates: N36°, E42°

SRTM3N36E043V1 Coordinates: N36°, E43°

SRTM3N37E043V1 Coordinates: N37°, E43°

SRTM3N37E042V1 Coordinates: N37°, E42°

Additionally:

Bing Basemap, also available for free.

Urban areas and vegetation

Landsat 8 image were used to visually delineate urban and vegetated areas using ArcGIS software. First the image was optimized using the *Histogram Equalization*. Next all urban areas and existing vegetation were mapped based on (1) a false colour composite with the band combination 5/4/3 and (2) a calculated NDVI image, which highlights vegetated areas (Figure 3-3). Additionally, very high resolution images provided by Bing Basemap were useful to map urban areas and the existing vegetation.

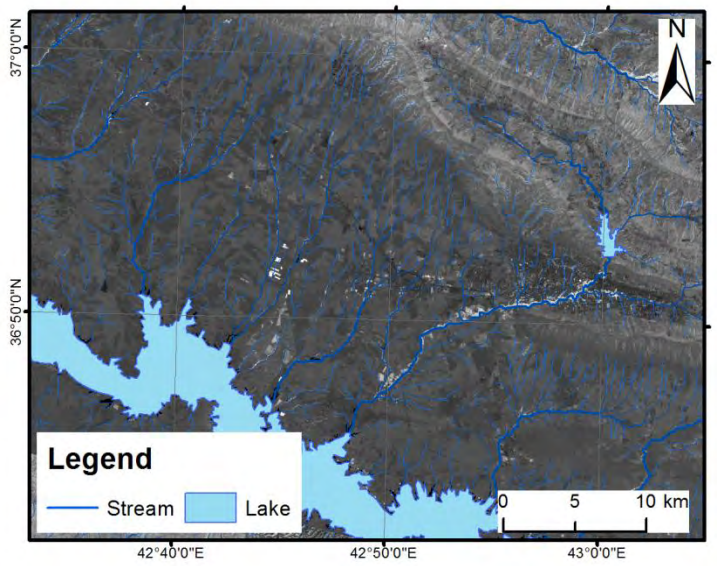

Figure 3-3: NDVI background image and the drainage system (highlighted in blue) of Domeez testsite

Lithological mapping

Different lithological units were delineated based on the Landsat 8 image with the band combination 7/6/3 (Figure 3-4), whereas the band combination has been identified by trial-and-error. Additionally, the SRTM digital elevation model has been proven useful to extract joints and fold axes.

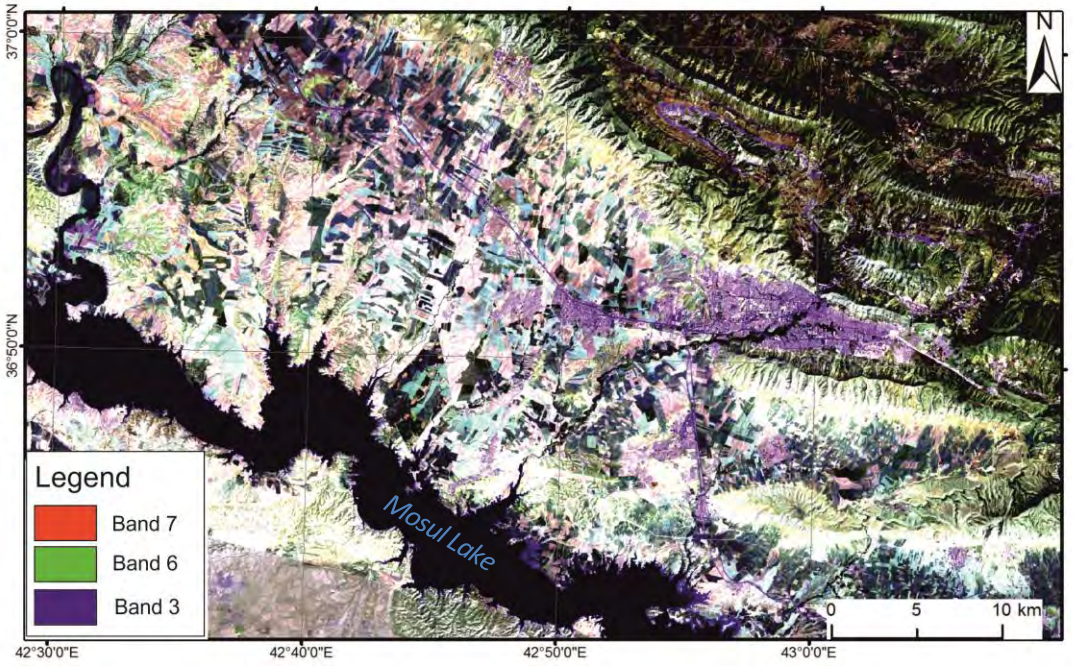

Figure 3-4: Landsat 8 image of Domeez, band combination 7/6/3.

The area north of the Mosul Lake is covered by quaternary sediments (cf. Figure 3-4). They superimpose a fold belt further to the north. Here, 7 different sedimentary rock units were differentiated based on different spectral properties in the Landsat 8 image. The band ratio 4/2 highlights iron minerals, which are shown in Figure 3-5 (light unit). A clay-rich zone is located in the centre of the fold as indicated by high intensities in the band ratio 7/6, (Figure 3-6). For water exploration the location of this clay zone is important as it can be interpreted as an

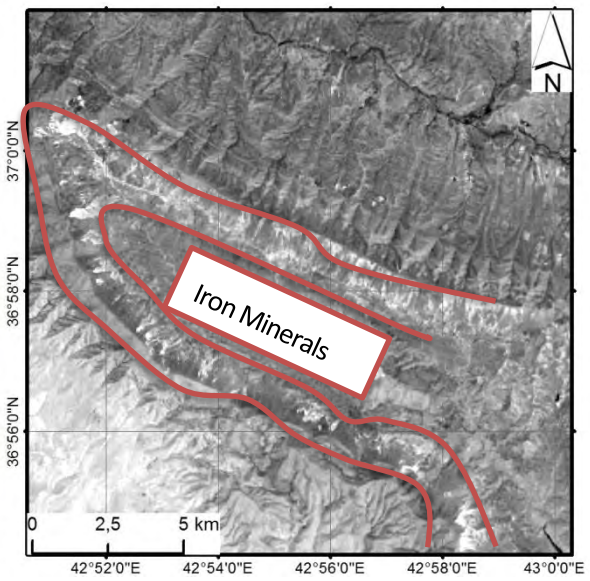

Figure 3-5: Band ratio 4/2

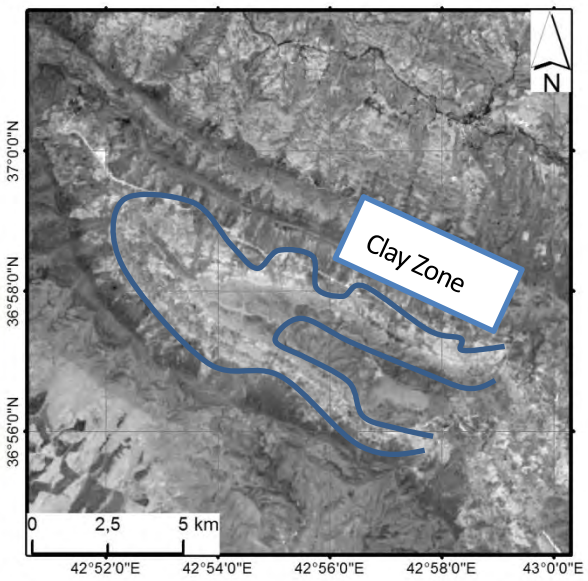

Figure 3-6: Band Ratio 7/6

impervious bed.

Strike and dip measurement

Strike and dip of geologic layers were determined by the ArcGIS tool developed by Kneissl et al. (2010) using the Landsat 8 image and the DEM. For tool description see section 2.3.2.1. Figure 3-7 illustrates the application of this tool, resulting in a dip of 26° and a dip direction of 226°. The intersection between the calculated plane and the DEM is calculated to verify the goodness of fit visually. The red dotted area represents the part of the calculated plane above the DEM surface

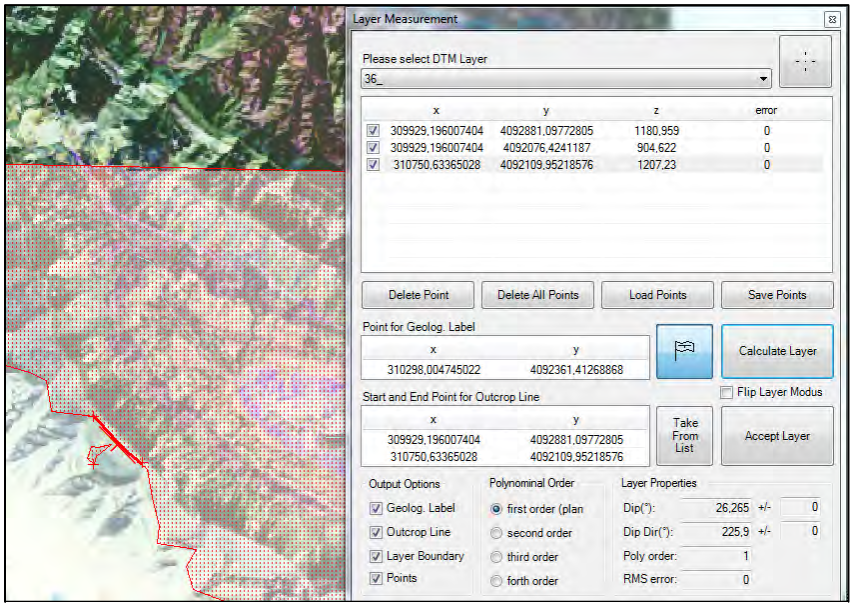

Figure 3-7: Strike and dip measurement tool for ArcGIS

Drainage Network

The drainage network was calculated using the ArcGIS Spatial Analyst toolbox, as described in section 2.3.3.1. Using the 90 m DEM as input data the most demonstrative results were obtained by calculating the catchment size value of 0.8 km² (cf. Figure 3-9). This means streams with a catchment area greater than 0.8 km² are highlighted. The drainage system of this area can be interpreted as *parallel drainage system* in the quaternary sediments. *Parallel* drainage (Figure 3-8) is found on uniform materials, but on landscapes that have pronounced regional slopes. Parallel drainage resembles the dendritic pattern but is distinctive by its elongated form derived from the increased typographic slope (Campbell and Wynne 2011).

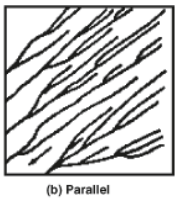

Figure 3-8: Sketch of parallel drainage pattern Campbell and Wynne (2011).

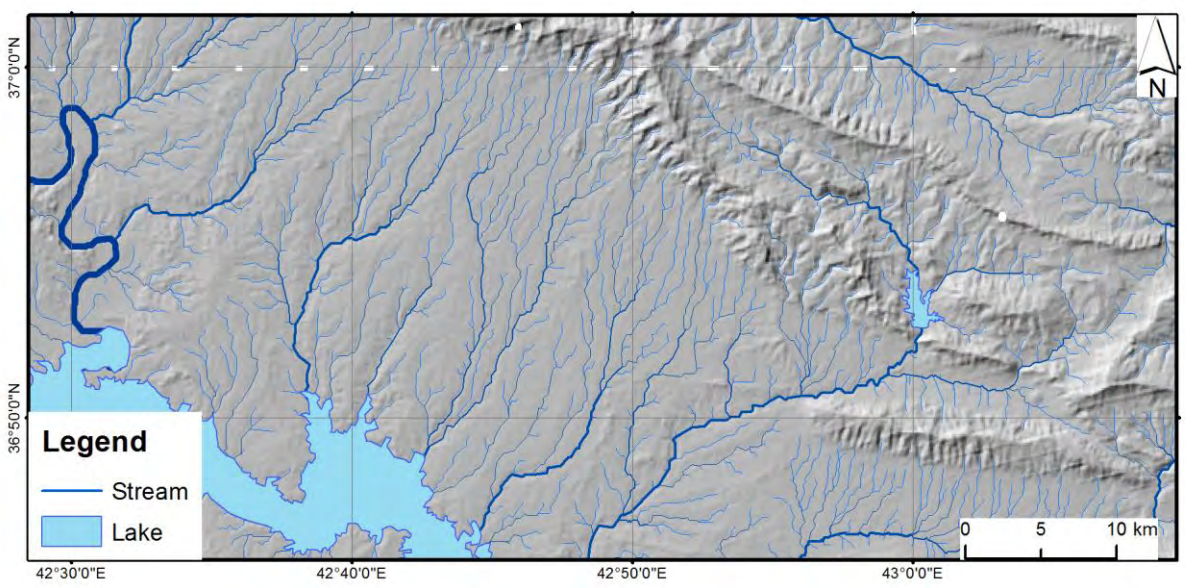

Figure 3-9: Drainage Network

Results

Figure 3-10 shows the resulting geological map combining the analysis results described above.. The map is based on remote sensing data only. A possible water exploration area is marked with a blue ellipse. Profile A (Figure 3-11) and Profile B (Figure 3-12) were prepared based on the strike and dip measurements from the DEM and the geological map, but without field validated borehole data. In folded sediments successful water exploration is most probable when drilling in a syncline, where flow lines are convering and is likely to hit a water bearing formation. Due to the possible clay–rich aquitards, it is justified to drill into litholgical unit 5 or 6 above (cf. Figure 3-11). This suggested exploration area is also located upstream from the refugee camp.

In this test site, remote sensing data is useful to determine the geological structure. However, field work would comprise a determination of the composition of the individual sedimentary units and provides a general validation of the map.

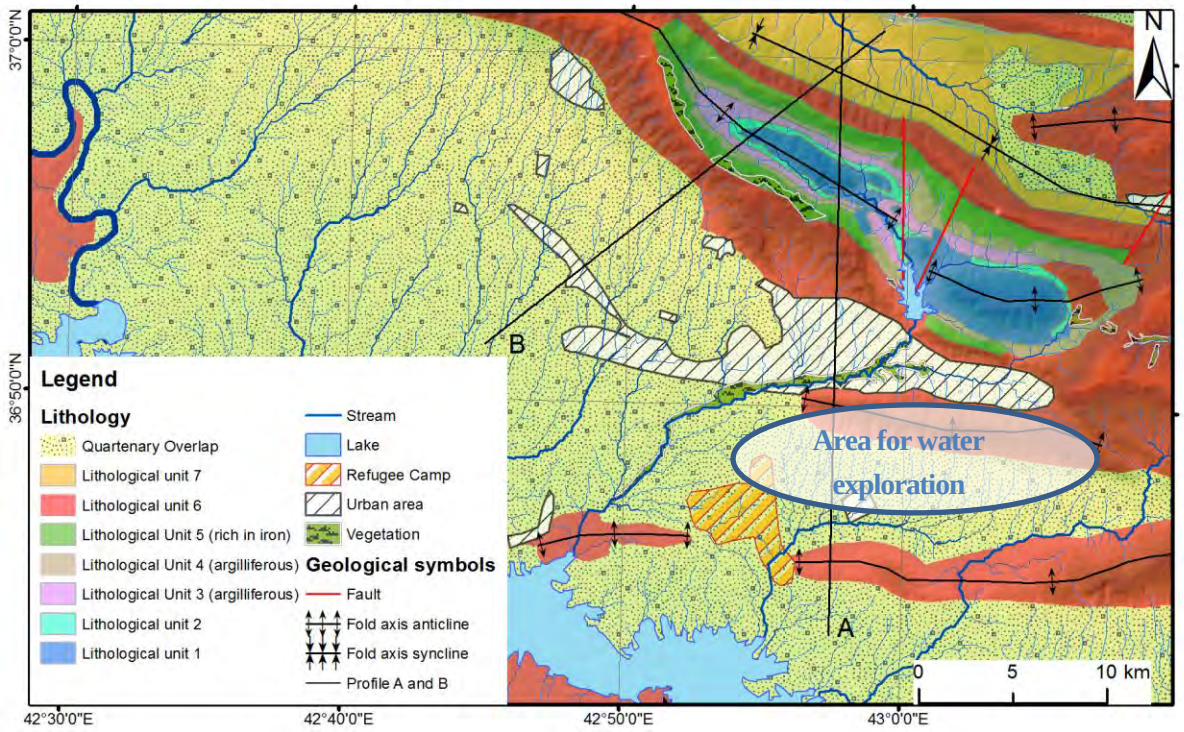

Figure 3-10: Geological map based on remote sensing data

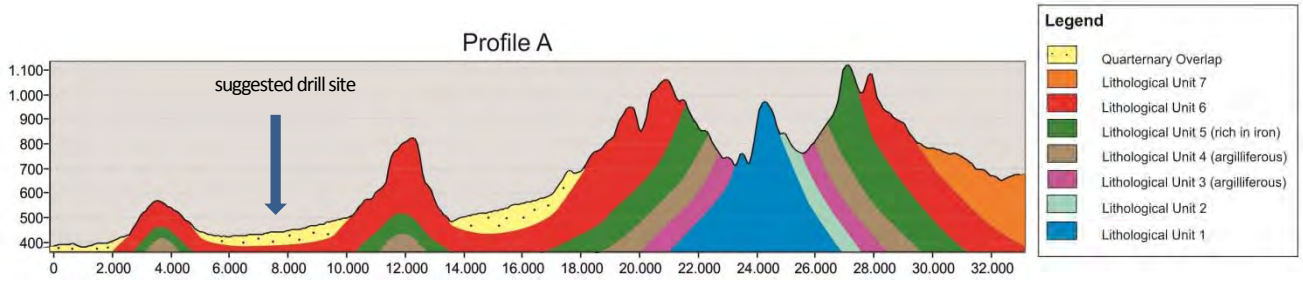

Figure 3-11: Profile A with possible drill site marked by arrow

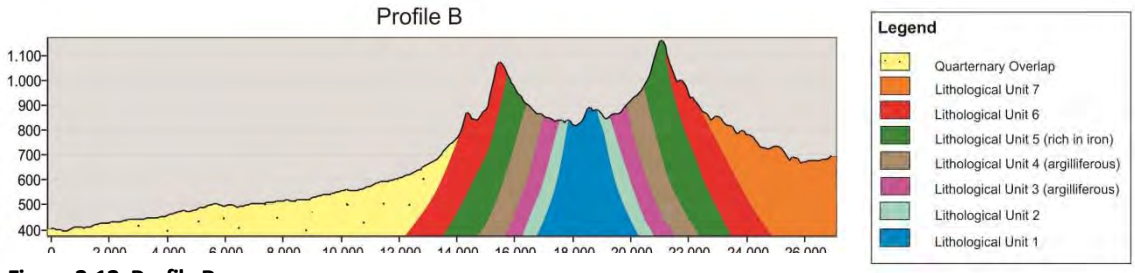

Figure 3-12: Profile B

3.3 RAURIS

Overview

This test site is located in the Austrian Alps, within the province of Salzburg and close to the small town Rauris (Figure 3-13), which is located around 120 km south of the city of Salzburg. The size of the area is 8,5 km² and the surface elevation ranges from 1550 m up to 2550 m above sea level. It is an alpine region and approximately 30 % of the surface is forested. The other 70 % of the area are located above the tree line and are mostly covered by talus and glacial sediments. Geologically this area belongs to the *Tauern window* and is characterized by two lithological units, namely the *Zentralgneis* (gneiss) and *Schieferhülle* (shale). The test site was chosen as an example for crystalline lithology under wet/dry seasonal climate conditions. Although the climate would be characterized as humid from the hydrological point of view, from the hydrogeological perspective the classification fits the seasonal variation in groundwater recharge. The Zentralgneis is the main unit for possible water extraction, because it contains wide open fractures.

Figure 3-13: Overview map (ArcGIS)

Data

Landsat 8 image of the 03. August 2013 (not snow covered), image number: LC81920272013215LGN00

DEM SRTM 3 arcsecond, 1. February 2005,

SRTM3N47E013V1 / Coordinates**:** N47°, E13°

SRTM3N47E012V1 / Coordinates: N47°, E12°

Additionally:

Bing Basemap in ArcGIS with a spatial resolution of 30 cm

DEM with 10 m ground sampling distance (GSD) provided by SAGIS (14. April 2011)

Structural mapping

Due to the small size of this research area, an additional elevation model with a resolution of 10 m was used. Figure 3-14 shows the comparison between the two elevation models. On a mapping scale of 1:60.000 the resolution of the SRTM 3 arcsecond data is insufficient as an extraction of lineaments and other structures is not possible, whereas the main joints are discernible in the 10 m DEM (cf. Figure 3-14). The orientation of the main joints ranges from N-S to NNW-SSE, which nearly fits together with the results of the field work, with a main joint orientation of N-S.

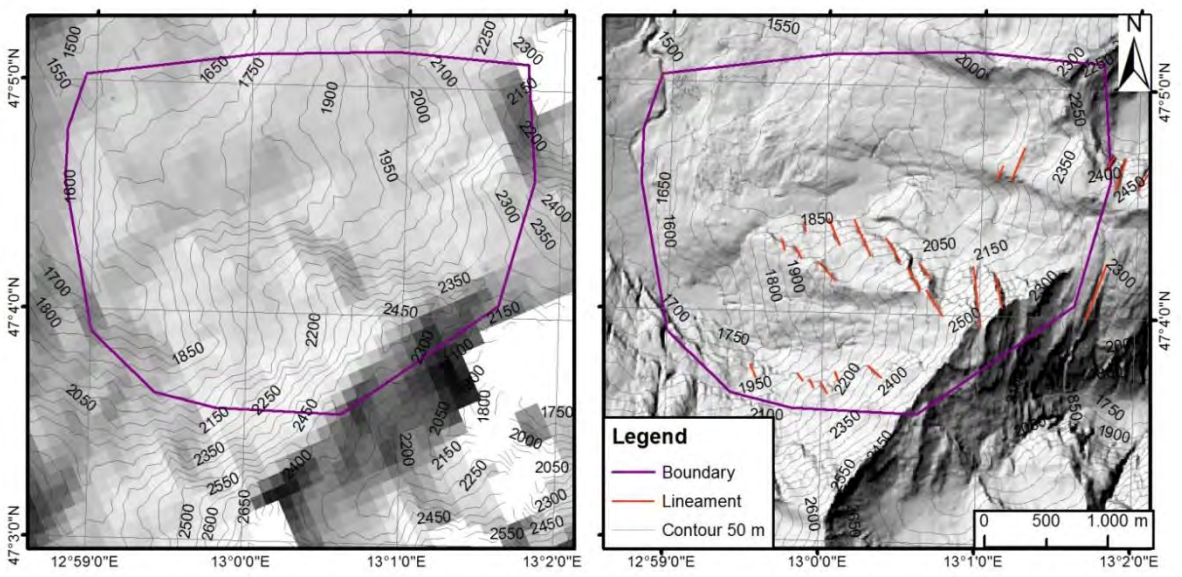

Figure 3-14: Elevation Models with resolution of 90 m (left) and 10 m (right).

Lithological mapping

Remote sensing results

To delineate different lithological areas, a Landsat 8 image (Figure 3-15, left image) with a band combination of 7/5/3 and the 10 m DEM were used. This band combination was useful for mapping geological units and vegetation within this area. Forested areas appear in dark green and parts above the tree line, which are mostly covered by glacial sediments, appear in light in green, bedrocks in purple. However, areas covered with forests and sediments make it difficult to distinct certain lithological units. In the center of the area a pore aquifer can be identified, unveiled in the DEM as a flat surface.. Spring zones were mapped using a very high resolution image provided by Bing Map.

Field work results

The geological field map (Figure 3-15, right image) shows the pore aquifer and the spring zones, which resemble the results of the remote sensing image interpretation. The field work has revealed that the pore aquifer is a fluvial deposit, where the grain size ranges from 1 mm to 40 cm. The field work allows a distinction between the *Zentralgneis* and *Schieferhülle*, whereas a further differentiation of the outcrops of bedrock in the remote sensing data was not possible. This distinction is relevant for hydrogeological purposes as the *Zentralgneis* contains open fractures that transport water, while the *Schieferhülle* does not. Additionally, deposits of a massive landslide are located in the forested areas, which can be subdivided into three zones. This landslide deposit is not recognizable in the remote sensing data.

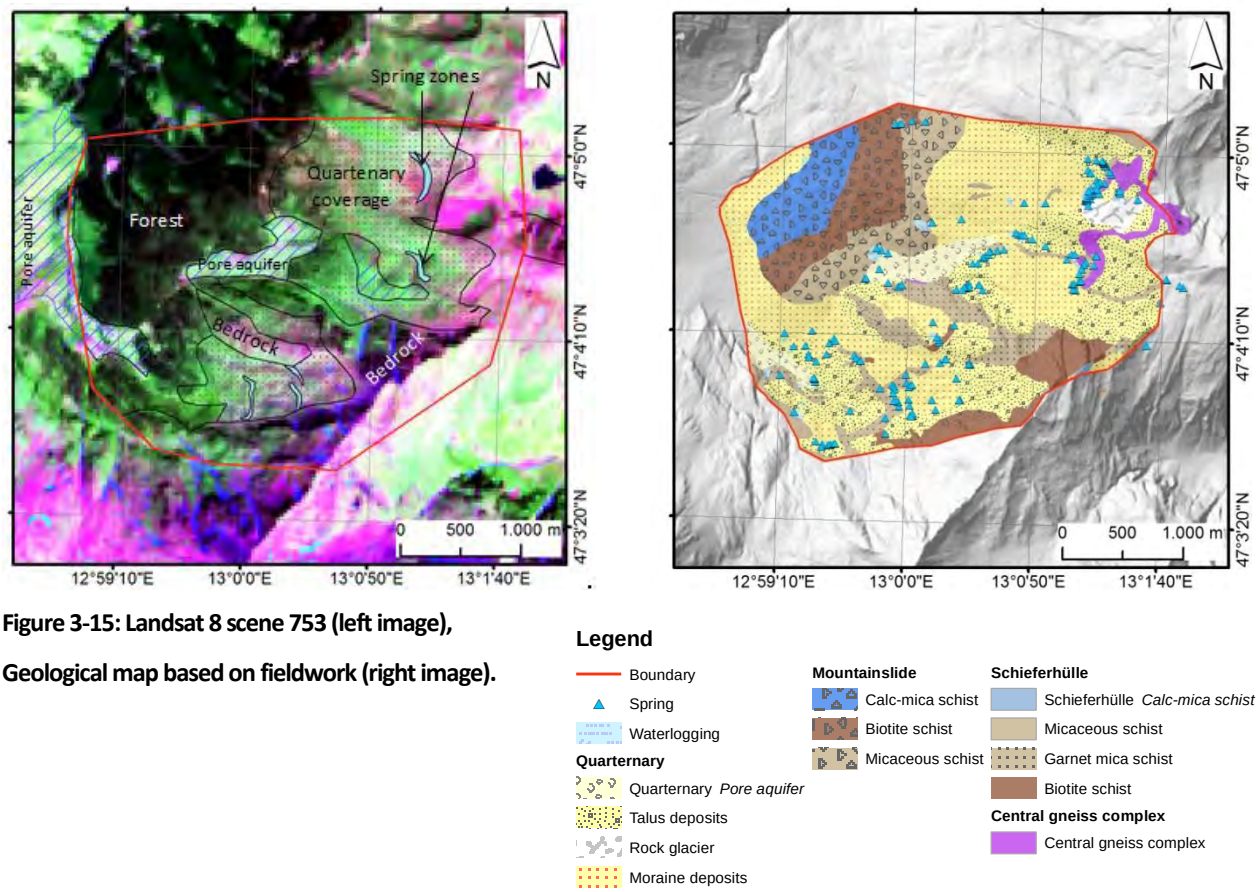

Figure 3-15: Landsat 8 scene 753 (left image), Geological map based on fieldwork (right image).

Drainage network

The drainage network was calculated with the ArcGIS Spatial Analyst toolbox (cf. section 2.3.3.1) using the 10 m DEM. Using this scale the drainage area of 0.1 km² leads to the most plausible results, illustrated in Figure 3-16. The result shows that the calculated area of spring zones fits well with the manual delineation based on field work and Bing Maps images. Figure 3-16 (right) shows the automatically delineated three different catchments, their drainage network and watersheds. This type of analysis is important to assess the influence of a source of contamination on surface water or well.

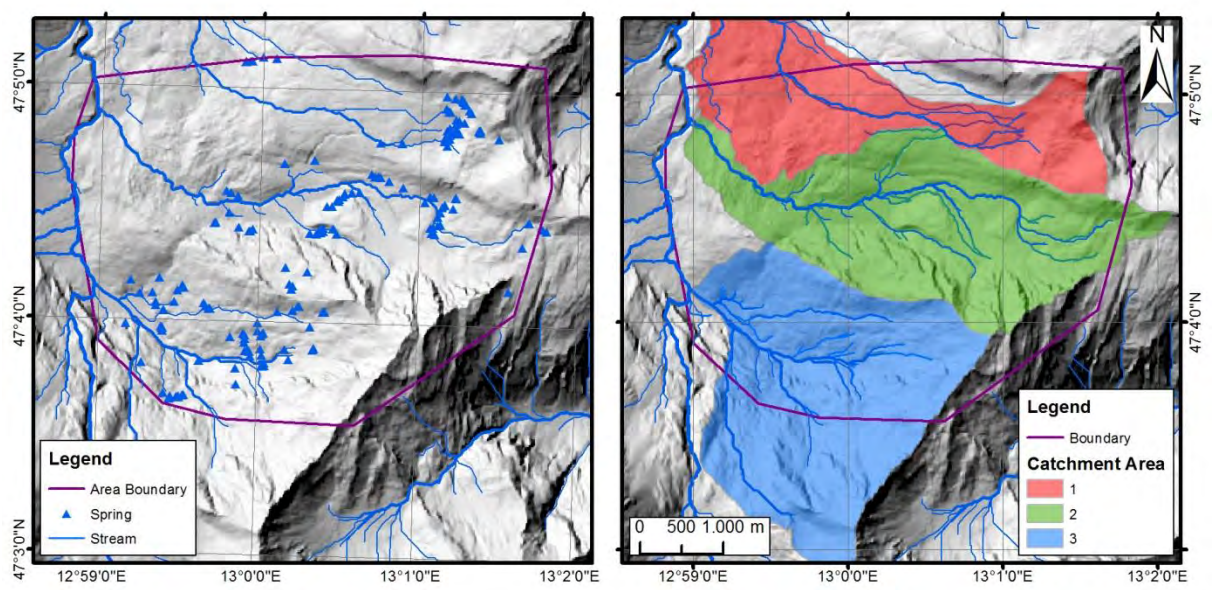

Figure 3-16: Drainage network / Catchment Areas

Conclusion

Based on the Landsat 8 image, the very high resolution imagery provided by Bing Maps and the 10 m DEM, it is possible to identify a pore aquifer and lithological units, but the bed rock aquifer of interest is not recognizable due to the sedimentary cover. If detailed geological maps are missing, these lithological units have to be determined in the field. Deriving the drainage system can be very helpful to find potential spring areas and to facilitate the field work, but it has to be kept in mind that it will not give information about the actual water flow.

3.4 NUBA MOUNTAINS

Overview

This study area, covering about 170 km², is located in the Nuba Mountains in Sudan, about 100 km north of the border to South Sudan (Figure 3-17). The region is characterized by metamorphic rocks and the climatic conditions are semiarid. As mentioned above, this area was selected as a representative for crystalline rock formations showing distinctive lineament structures, where lineaments have a high potential for groundwater exploitation. Methods developed and tested in this area should be transferable to other sites with similar geological setting in the wider area. In this study site, the focus was set on observing and extracting lineaments, rather than providing possible drill sites to supply a specific settlement with drinking water.

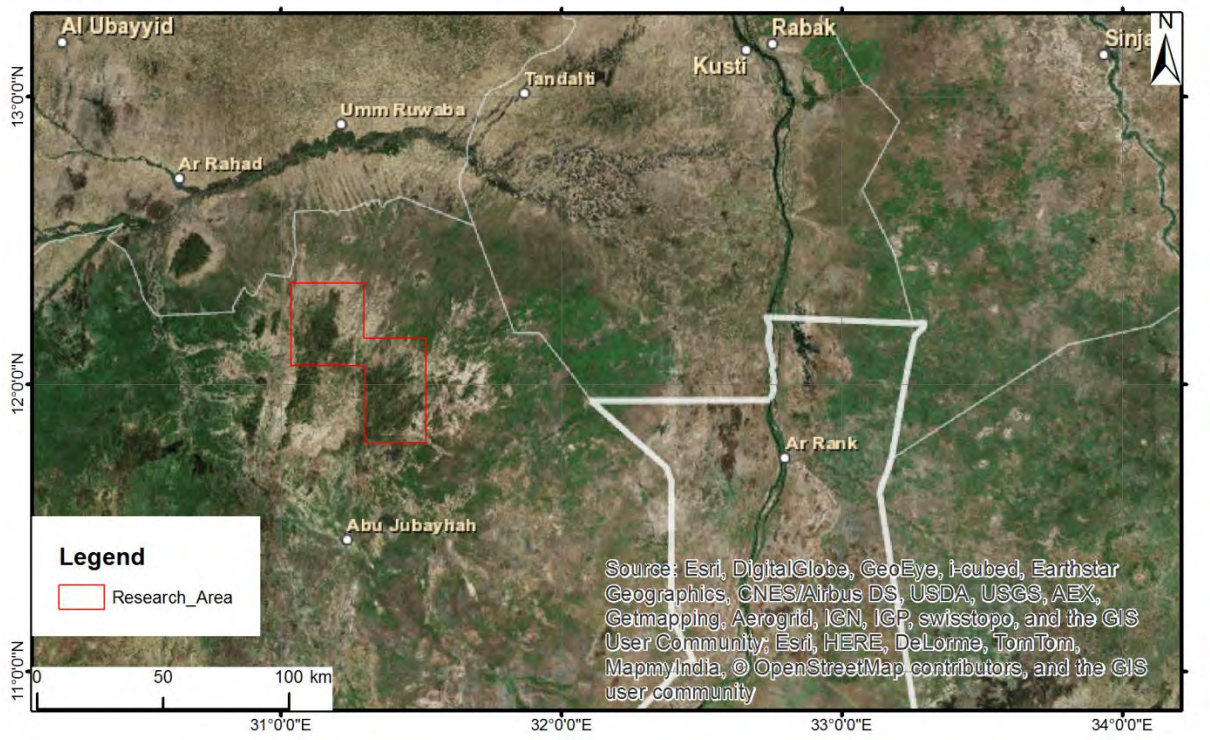

Figure 3-17: Areal map ArcGIS

Data

Landsat 8 image, 21. June 2014 (rainy season), image number LC81740522014172LGN00

Landsat 8 image, 28. January 2014 (dry season), image number LC81740522014028LGN00

DEM: ASTER GDEM 30 m

DEM: SRTM 3 arcsecond, 01. February 2005

SRTM3N12E030V1 Coordinates: N12°, E30°

SRTM3N11E030V1 Coordinates: N11°, E30°

SRTM3N12E031V1 Coordinates: N12°, E31°

SRTM3N11E031V1 Coordinates: N11°, E31°

Additionally:

Bing Basemap

Urban areas, Vegetation and Drainage Network

The vegetation was delineated based on a Landsat 8 images using a band combination of 5/4/3. Additionally, the NDVI was calculated for both Landsat 8 scenes covering the rainy season (Figure 3-18) and the dry season (Figure 3-19), where the vegetated areas are revealed by bright values. The two images show the difference in vegetation between rainy season and dry season. The region is sparsely populated and it was not possible to map the small settlements present in the area in this scale. Next, the drainage network was calculated with ArcGIS Spatial Analyst toolbox using SRTM 3 arcsecond DEM and a catchment area value of 0.8 km². The value was defined by trial-and-error and reveals demonstrative results.

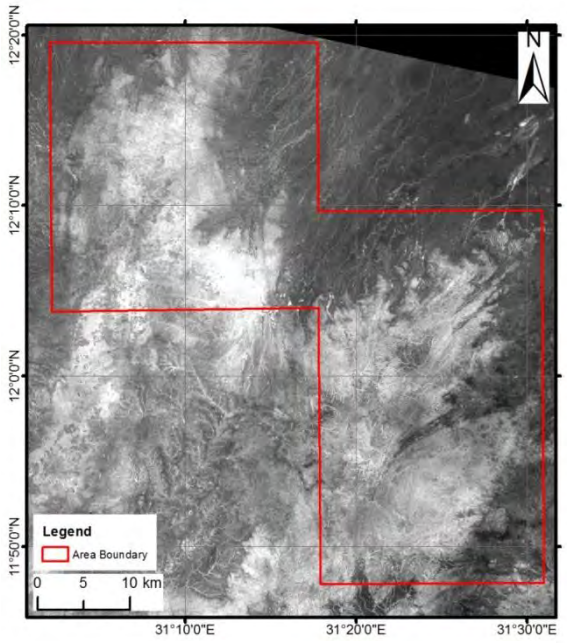

Figure 3-18: NDVI rainy season in June, 2014.

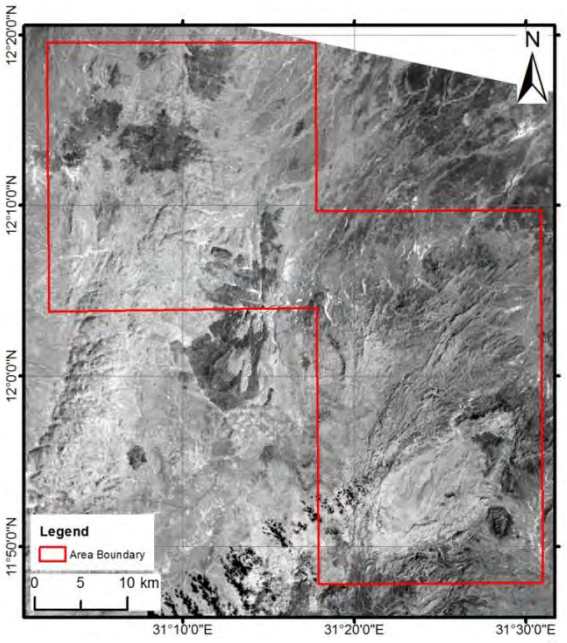

Figure 3-19: NDVI dry season in January, 2014.

Lithological mapping

Figure 3-21 shows the Landsat 8 image ofJune 2014 with a band combination of 7/5/2. The image was optimized in ArcGIS using the *Histogram Equalization* tool Both satellite scenes were suitable for lithological mapping and showed no perceiveable differences in image interpretation. The lithological units were differentiated, based on different spectral properties of the Landsat scene: white and purple are overlying sediments, light green are

granite or gneiss dome, which are located in the south of the research area. This dome can be distinguished from other lithological units, due to its characteristic round structure.

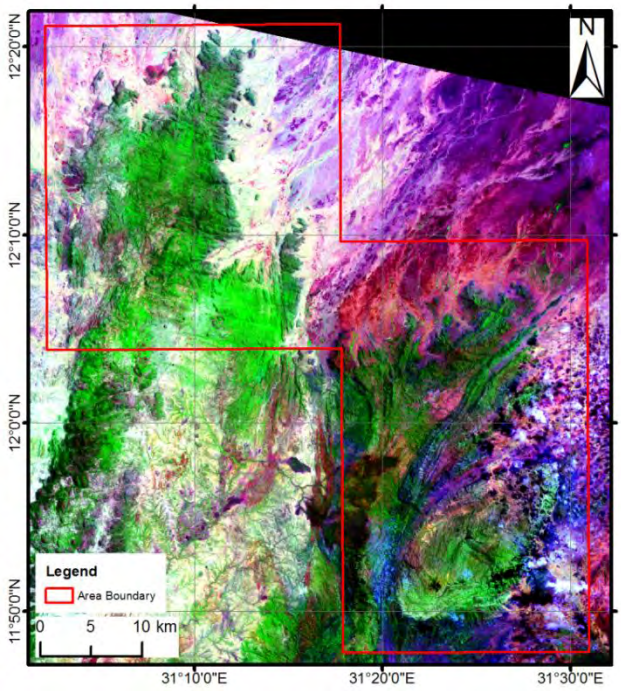

Figure 3-20: Landsat 8 scene (7/5/2)

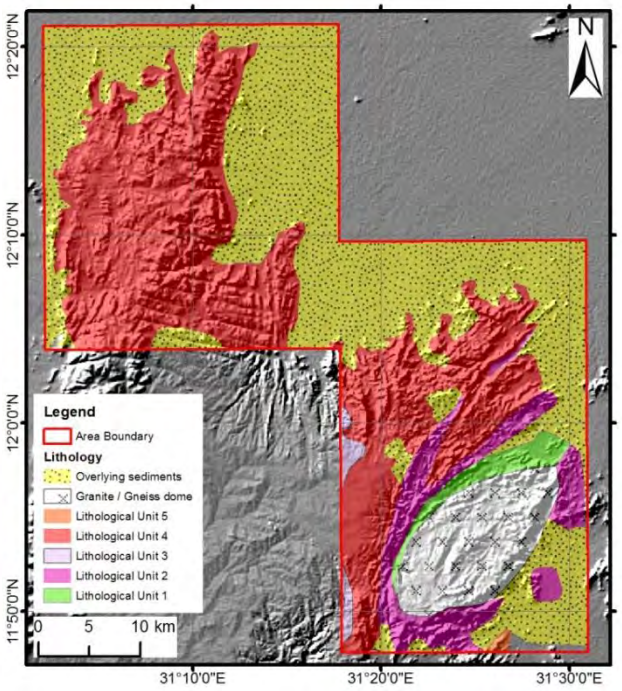

Figure 3-21: Mapped litological units

Lineament Mapping

The structural inventory of the study area consists of (at least) two different sets of lineaments that represent different stages of the geological evolution of the domain (Figure 3-22). Curved lineaments are predominantly observed at a large shear zone located at sub-domain 1. The shear zone developed at high grade metamorphic conditions and shows ductile deformation. A second set of structures is characterized by a low plan view curvature and indicate a latter tectonic phase accompanied by pervasive brittle deformation. Brittle structures occur frequently within the entire study region (Sub-domain 1 and Sub-domain 2) but the discrimination between intersecting brittle and ductile structures by remote sensing is challenging. However, Sub-domain 2 is several tens of kilometers apart from the ductile shear zone and most lineaments represent the morphological expression of the brittle tectonic phase. Therefore we contrast Sub-domain1 and Sub-domain 2 with predominantly brittle and ductile structures, respectively. Figure 3-23 shows a detailed view on sub-domain 2 and possible areas for water exploration along the lineaments.

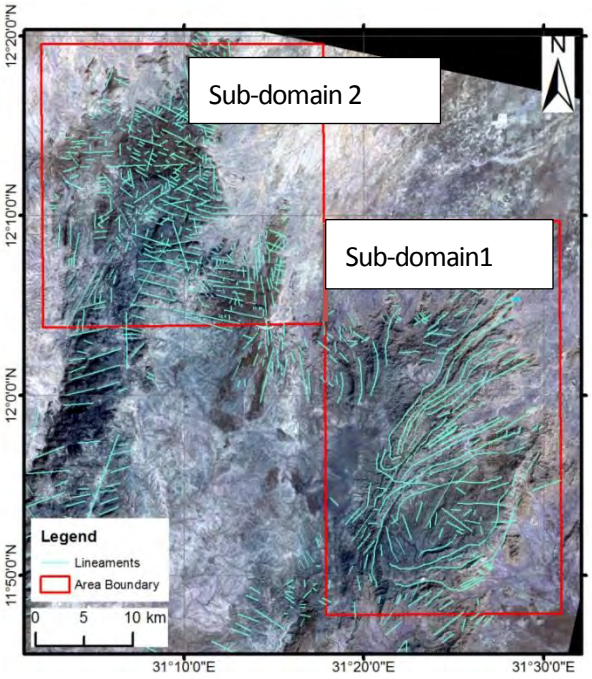

Figure 3-22: Mapped Lineaments

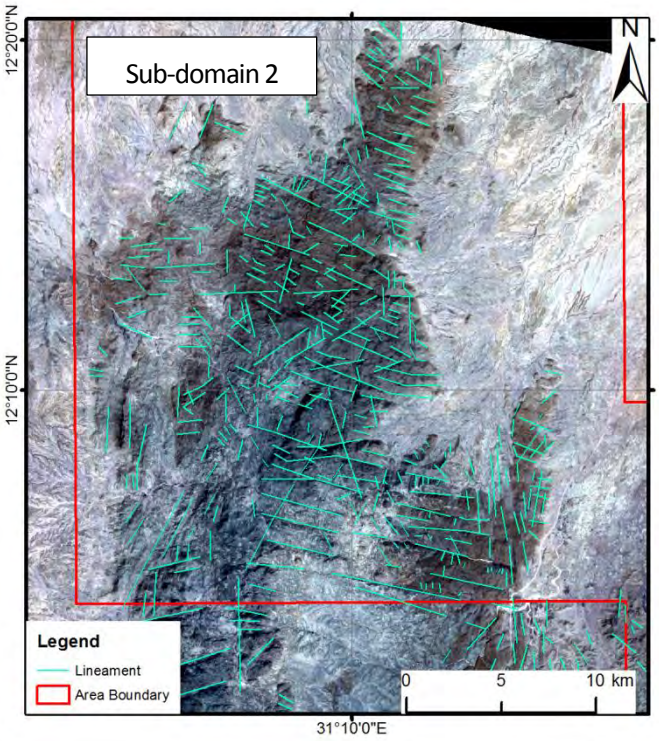

Figure 3-23: Area of brittle deformation and probable drill points

Figure 3-24 shows the strike of the Lineaments of sub-domain 2. The main directions are N-S and WNW-ESE. The number of delineated lineaments is 447.

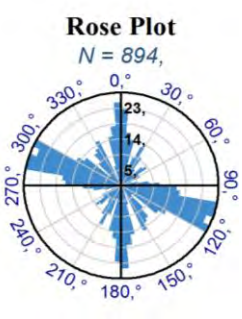

Figure 3-24: Rose plot of lineaments in sub-domain 2.

Conclusion

It is difficult to define lithological units in this complex metamorphic area but it is well suited for manual digitization of lineaments. The lineament analysis of remote sensing data reveals the complex deformation history of the Nuba Mountains with a ductile and a brittle phase. The main orientations of lineaments are WNW-ESE and N-S. Ground water exploration in this area should focus on the intersection of brittle structures.

3.5 PAOUA, CENTRAL AFRICAN REPLUBLIC

The study for Paoua in the Central African Republic was conducted together with Hydrogeologists without Borders UK, who had been asked by MSF France first assess the hydrogeological setting and then supervise the drilling and well construction for an MSF hospital and MSF living quarters. For the desk study, Z_GIS produced the maps, while HWB-UK wrote the report.

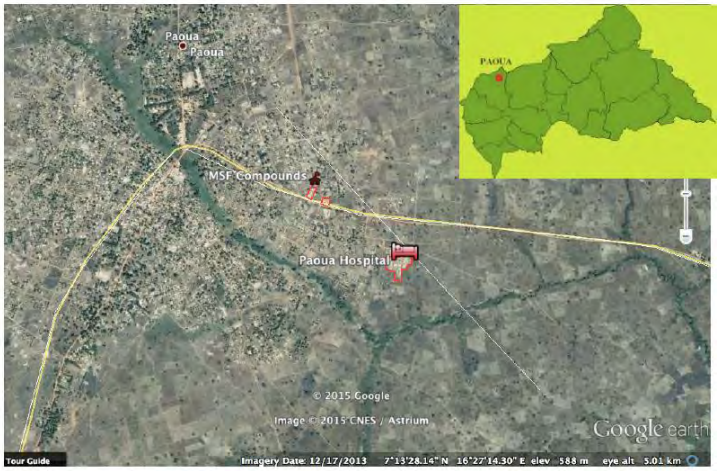

Figure 5: Overview to Paoua Town, CAR

The geology in this area is dominated by Precambrian-aged granitic rocks; soil cover and vegetation make a lithological mapping by remote sensing impossible. Therefore, the objective was to prepare a collection of maps to support the field work in the best possible way. The available geological map indicated lineaments in a NNW-SSE-directions and NNE-SSW-directions, which could also be observed in the DEM and a local outcrop:

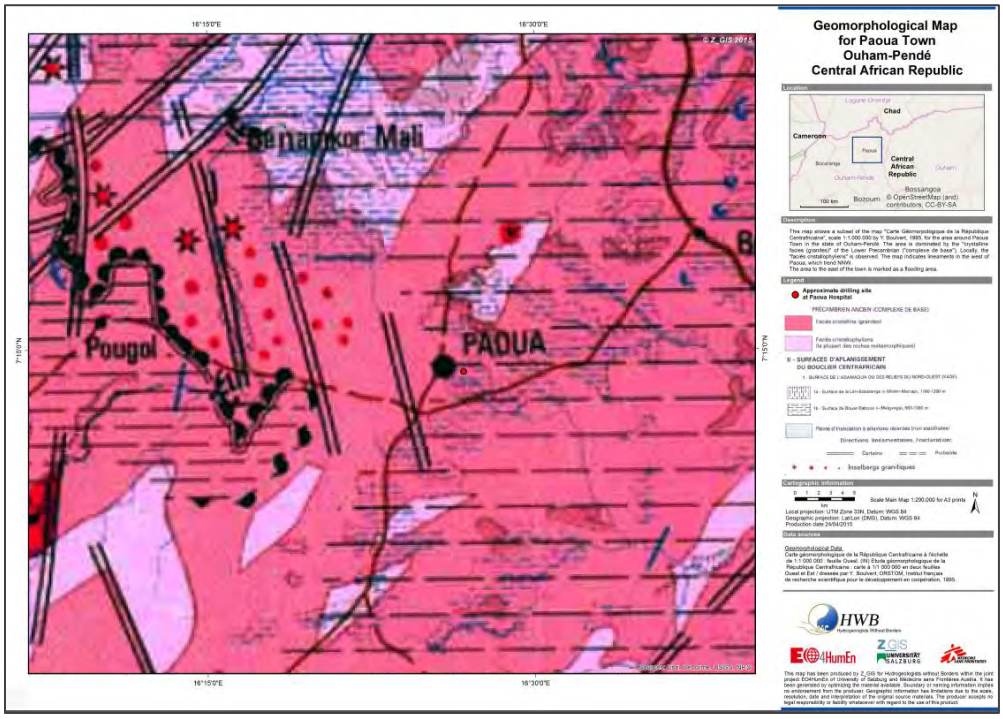

Figure 6: Extract of geomorpholigical map at scale 1:1.000.000, Insitut Francais de Recherche Scientifique pour le Developpement en Cooperation, 1995; SRTM-DEM or the area; local outcrop of granite (photo: Geraint Burrows, HWB-UK)

Also, satellite maps, topographic maps and road maps based on OpenStreetMap were produced to help orientation in the field.

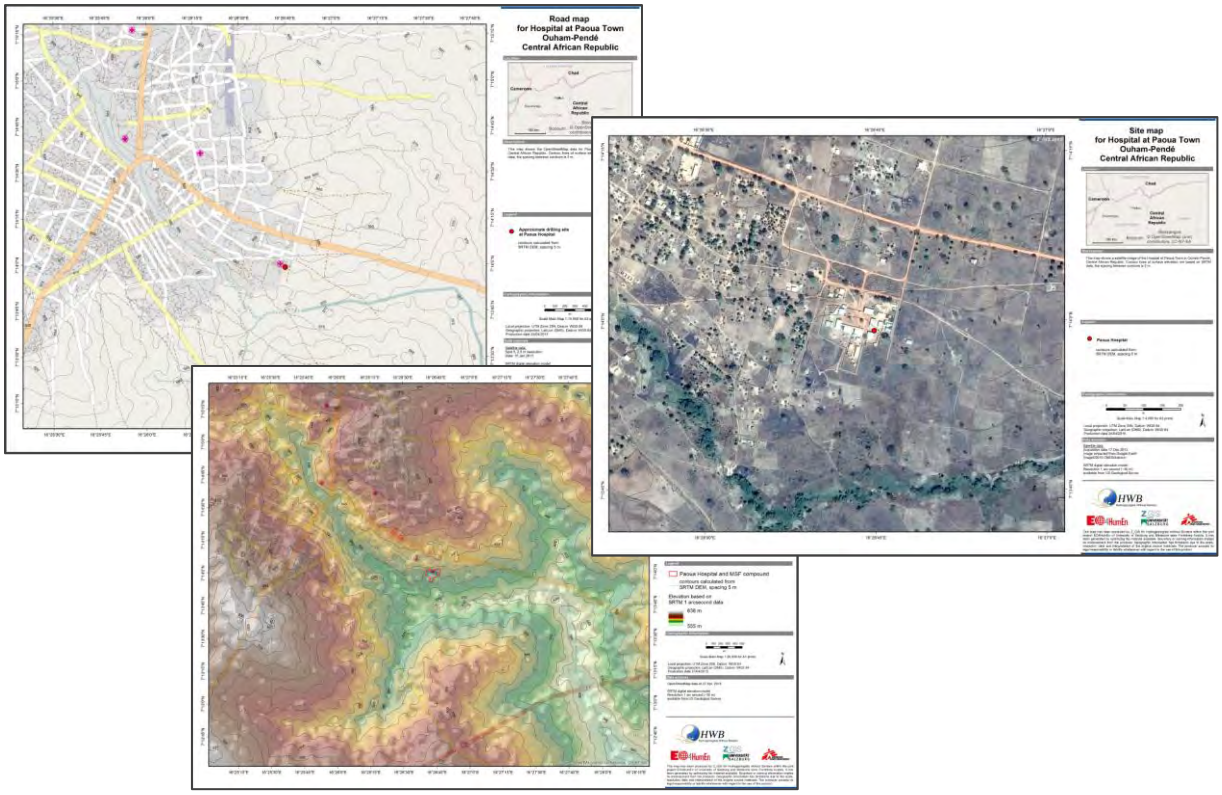

Figure 7: Road map, satellite map and topographic map produced before field work for orientation.

Once on site, it was also possible to acquire locations of existing boreholes with yields and partly with water levels and the thickness of the weathered rock, which indicated that a sufficiently thick saturated weathered layer would be encountered at the locations for drilling.

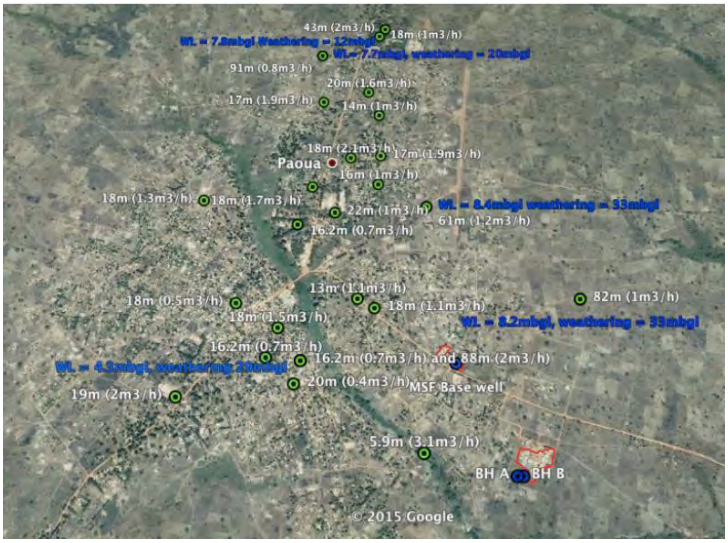

Figure 8: Borehole locations with yields, and locally WL and depth to hard rock, acquired from local groundwater authority. (Map compilation by HWB-UK).

The location for the boreholes was confined to the MSF compound, leaving little choice for the exact placement. To pinpoint the borehole placement, several transects of electrical sounding were conducted to locate a geological structure parallel to those visible in the geological and topographic maps in order to maximize the expected yield.

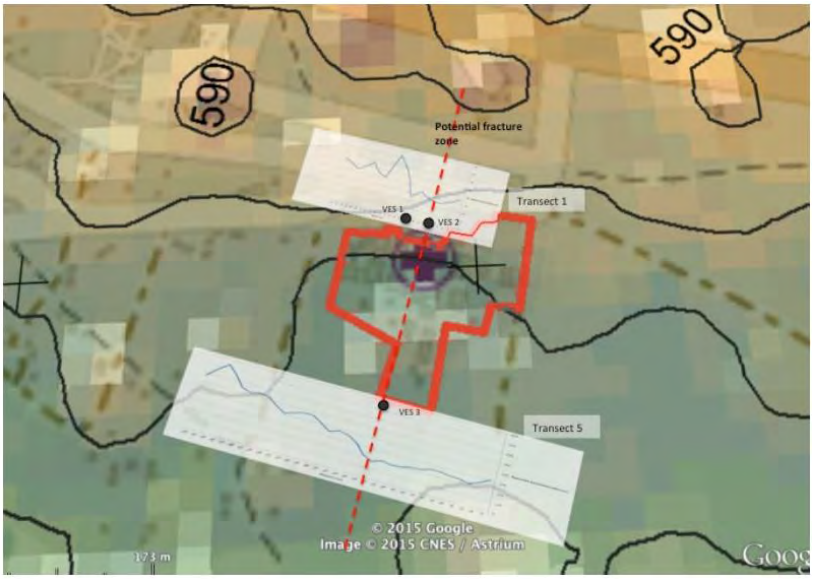

Figure 9: Geoelectrical profiles at MSF hospital, together with contour lines from SRTM

Finally, two successful boreholes were constructed at the MSF hospital and the MSF compound delivering much higher yields than required (4 m³/h and 2.25m³/h).

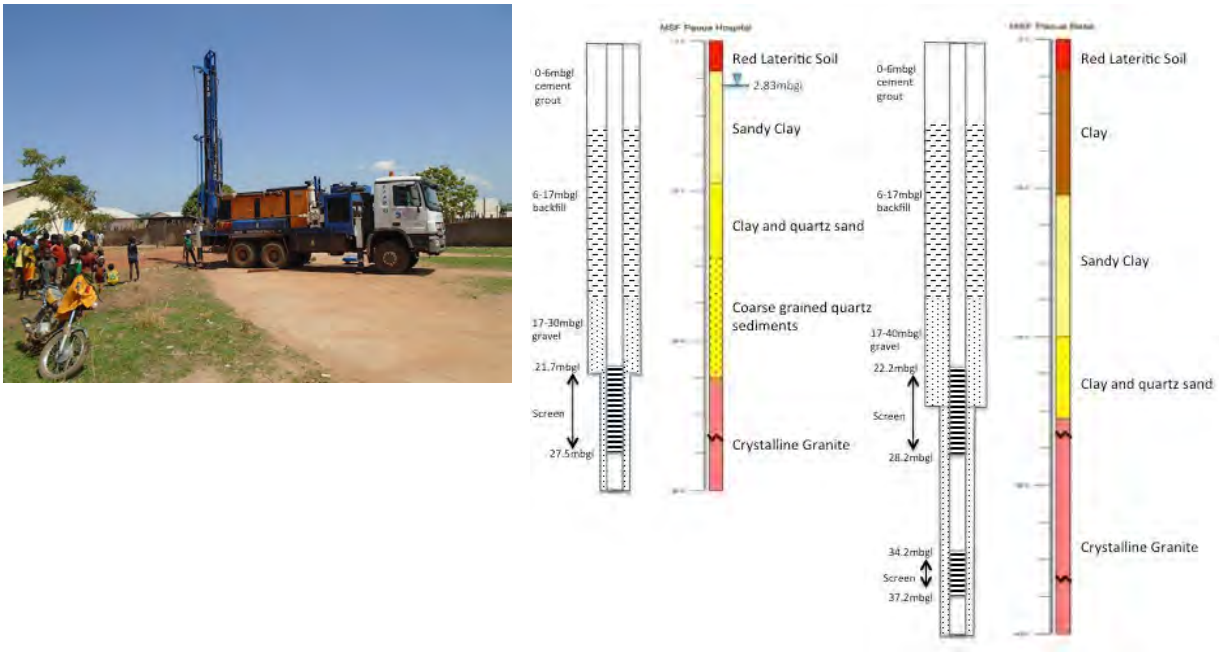

Figure 10: drilling rig, borehole logs and well construction plan

In this case study, the remote sensing itself did not deliver the single, crucial information for a successful termination of this drilling project, but it helped getting the overall picture and creating an overview to the existing data. The most important factor was the good cooperation between remote sensing/GIS personnel at Z_GIS, the local supervision by the hydrogeologist from HWB-UK (now renamed to Groundwater Relief (www.groundwater-relief.org) and the professional skills and equipment of the drilling company.

Literature

Baghdadi, N., M. Aubert & M. Zribi (2012) Use of TerraSAR-X Data to Retrieve Soil Moisture Over Bare Soil Agricultural Fields. *IEEE Geoscience and Remote Sensing Letters,* 9**,** 512-516.

Baghdadi, N., P. Camus, N. Beaugendre, O. M. Issa, M. Zribi & J. F. Desprats (2011) Estimating surface soil moisture from TerraSAR-X data over two small catchments in the sahelian part of Western Niger. *Remote Sensing of Environment* 3**,** 1266-1283.

Campbell, J. B. & R. H. Wynne. 2011. *Introduction to Remote Sensing*. Guilford Press.

Fletcher, K. 2012. Sentinel-2: ESA's Optical High-Resolution Mission for GMES Operational Services (ESA SP-1322/2 March 2012). ed. ESA. Noordwijk: ESA Communications

Gupta, R. P. 1991. *Remote sensing geology*. Springer-Verlag.

Kneissl, T., S. van Gasselt & G. Neukum. 2010. Measurement of Strike and Dip of Geologic Layers from Remote Sensing Data — New Software Tool for ArcGIS. In *41st Lunar and Planetary Science Conference*, 1640. Woodlands, TX: LPI.

Kseneman, M., D. Gleich & B. Potočnik (2012) Soil-moisture estimation from TerraSAR-X data using neural networks. *Machine Vision and Applications,* 23**,** 937-952.

Langguth, H.-R. & R. Voight. 2004. *Hydrogeologische Methoden, 2. Auflage*. Springer-Verlag, Heidelberg.

Meijerink, A. M. J., D. Bannert, O. Batelaan., M. W. Lubczynski & T. Pointet. 2007. *Remote Sensing Applications to Groundwater*. UNESCO. http://unesdoc.unesco.org/images/0015/001563/156300e.pdf (last accessed 20.09.2014).

Prost, G. L. 2002. *Remote Sensing for Geologists: A Guide to Image Interpretation*. Taylor & Francis.